The Kinematics of a Midlatitude, Continental Mesoscale Convective System and Its Mesoscale Vortex

JASON C. KNIEVEL AND RICHARD H. JOHNSON

Department of Atmospheric Science, Colorado State University, Fort Collins, Colorado

(Manuscript received 4 April 2001, in final form 28 November 2001)

ABSTRACT

The authors present a unique, scale-discriminating study of the environment-relative circulations within a mesoscale convective system (MCS) and mesoscale convective vortex (MCV). The MCS, a leading convective line and trailing stratiform region that became asymmetric, passed through the National Oceanic and Atmospheric Administration (NOAA) Profiler Network (NPN) in Kansas and Oklahoma on 1 August 1996. The MCV appeared in the MCS's stratiform region just prior to the system's mature stage and grew to a depth of over 12 km as the MCS dissipated. The MCV did not apparently survive to the next day.

A spatial bandpass filter was used to divide observed wind into a component that was predominantly synoptic background wind and a component that was predominantly a mesoscale perturbation on that background wind.

A mesoscale updraft, mesoscale downdraft, and divergent outflows in the lower and upper troposphere were evident after the synoptic background wind was removed, so these four circulations were internal and fundamental to the MCS.

The mesoscale perturbation in wind in the middle troposphere extended farther behind the MCS than ahead of it, consistent with analytic studies and numerical simulations of gravity waves generated by heat sources characteristic of MCSs with leading convective lines and trailing stratiform regions.

Deepening of the MCV appeared to be reflected in the vertical wind shear at the vortex's center: as the MCV strengthened, the mesoscale shear through its lower part decreased, perhaps as wind became more vortical at increasing altitudes. Mesoscale and synoptic vertical shears were of similar magnitude, so an average of environmental soundings outside an MCS probably does not accurately represent the shear that affects an MCV. This suggests the need to reevaluate how the kinematical settings of MCVs are diagnosed.

1. Introduction

Mesoscale convective systems (MCSs) with extensive trailing stratiform regions often modify their local environments with strong, persistent mesoscale circulations rooted in deep layers of diabatic heating and cooling. Sometimes such circulations include a mesoscale convective vortex (MCV). In this paper we recount research in which we applied a bandpass filter to data from the National Oceanic and Atmospheric Administration (NOAA) Profiler Network (NPN) in order to diagnose the mesoscale, environment-relative circulations within an MCS and the MCV it generated. The MCS traversed Kansas and Oklahoma on 1 August 1996 and comprised a leading convective line and a trailing stratiform region, so all our commentary herein applies to this mode of MCS, although there are others (Houze et al. 1990; Parker and Johnson 2000).

Corresponding author address: Dr. Jason Knievel, Mesoscale Research Group, National Severe Storms Laboratory, 3450 Mitchell Lane, FL3, Boulder, CO 80301-2260.
E-mail: knievel@ucar.edu

a. Background

Because MCSs are large and long lived they impose upon tropospheric wind their own mesoscale circulations. These circulations often extend well beyond the clouds and rain of an MCS (Menard and Fritsch 1989; Pandya and Durran 1996), so what appears to be the environment in radar and satellite images may, kinematically, still be the MCS.

Convectively generated gravity waves and buoyancy rolls are the agents that transmit MCSs' circulations farthest (Nicholls et al. 1991; Mapes 1993). How far they are transmitted depends on the Rossby radius of deformation:

$$\lambda_R = \frac{NH}{(\zeta + f)^{1/2}(2VR^{-1} + f)^{1/2}}, \tag{1}$$

wherein N is the Brunt–Väisälä frequency, H is the scale height of the disturbance, ζ is the vertical component of the relative vorticity, f is the Coriolis parameter, and V is the wind's rotational component, of which R is the radius of curvature (Schubert et al. 1980; Frank 1983). It is generally appropriate to choose values for N, ζ, f, and V that are averaged over the region diabatically

heated by moist convection. In an environment of 100% relative humidity, rising air is heated by condensation as well as cooled by expansion, so N should be replaced by N_m, as explained by Durran and Klemp (1982).

How the atmosphere responds to heating by phase changes in water within a stratiform region depends partly on the horizontal size of the heated area compared with λ_R. When sources of diabatic heating are larger than λ_R, more energy is retained in balanced, vortical flow near an MCS than is transmitted to the far field by gravity waves and buoyancy rolls; the opposite occurs when sources of diabatic heating are smaller than the Rossby radius (Schubert et al. 1980; Mapes 1993). An MCS can shrink its local Rossby radius by saturating the stratiform region, which means a potentially lower-valued N_m replaces N, and by generating a vortical circulation, which increases $2VR^{-1}$ (Schubert and Hack 1982; Chen and Frank 1993). Therefore an MCS first triggers mostly propagative responses in the atmosphere, then as the system grows and matures it converts increasingly more energy into advective responses.

Gravity waves and buoyancy rolls are among the atmosphere's initial propagative responses to concentrated heating and cooling. Advective responses include mesoscale updrafts and downdrafts, part of convergent inflows and divergent outflows (buoyancy rolls contribute to inflows and outflows as well), and MCVs.

The advective part of a mesoscale updraft originates in a convective line. Ascent in a mesoscale updraft comes primarily from heating by deposition in dissipating, buoyant convective cores that move rearward from a convective line (Biggerstaff and Houze 1991). Rearward motion in a mesoscale updraft comes partly from high pressure in warm updrafts of a convective line, and partly from a line's vertical flux of rearward momentum (Gallus and Johnson 1992).

The advective part of a mesoscale downdraft originates in a stratiform region. A minimum in pressure forms in the middle troposphere at the front of a stratiform region when pressure hydrostatically decreases below the tops of tilted convective updrafts (LeMone 1983). A second minimum in pressure often forms behind the first when diabatic heating in a slanted mesoscale updraft surmounts diabatic cooling from precipitation (Brown 1979; Johnson and Gallus 1988). Both lows accelerate air from rear to front in a stratiform region.

Divergent outflow in the lower troposphere occurs when an evaporatively and sublimatively cooled mesoscale downdraft decelerates upon reaching the ground or a stable layer above the ground. Divergent outflow in the upper troposphere is due to a cold region of high pressure (Maddox et al. 1981; Cotton et al. 1989).

Large, long-lived MCVs of the kind generated on 1 August 1996 are less common circulations (Trier et al. 2000b). They are generally centered in the lower or middle troposphere with tangential wind speeds of orders 1–10 m s^{-1}, diameters of order 100 km, and lifetimes of orders 1–10 h. In the context of potential vorticity, one source for MCVs is the atmosphere's balanced response to diabatic heating within a stratiform region (Hertenstein and Schubert 1991). Diabatic heating energizes gravity waves that convey some energy to the far field and retain some energy in a local vortical circulation. As already mentioned, the partitioning of energy to the far and near fields is based on the size of the system compared with the Rossby radius, given by (1).

MCVs organize some MCSs on the mesoscale (Menard and Fritsch 1989; Brandes 1990; Raymond and Jiang 1990) and can serve as the primary dynamical link between serial MCSs (Raymond and Jiang 1990; Fritsch et al. 1994; Trier et al. 2000b). There is even growing evidence that MCVs over warm ocean water can be precursors of tropical cyclones (e.g., Bosart and Sanders 1981; Miller and Fritsch 1991; Harr et al. 1996).

Exactly why MCVs are less common than other mesoscale circulations in MCSs is not well understood, but vertical shear is a known factor. Climatologies by Bartels and Maddox (1991) and Trier et al. (2000a) and numerical simulations by Davis and Weisman (1994) and others demonstrated that MCVs are more likely to form in weak to moderate, rather than strong, vertical shear. Once an MCS generates its own circulations, vertical shear in its stratiform region is much different from that in the environment. Local relative vertical vorticity may also be much different from that in the environment because MCSs often form in negative synoptic-relative vertical vorticity (Cotton et al. 1989). (Henceforth, *vorticity* means *relative vertical vorticity*, and *divergence*, *convergence*, and *shear* mean *horizontal divergence*, *horizontal convergence*, and *vertical shear* unless otherwise stated.)

b. Objective and motivation

Our objective in this paper is to present the kinematics of a midlatitude, continental MCS and MCV from a unique perspective made possible by the spatial and temporal resolution of recently available data, and by a method of analysis in which mesoscale wind is separated from synoptic wind. This perspective allows us to pursue two points concerning the structure and evolution of MCSs addressed rarely, or not at all, in the literature.

The first point is the character of the MCS's mesoscale imprint on its environment. MCSs are commonly depicted in a storm-relative frame of reference, whereby the translational motion of an MCS is subtracted from observed wind. This approach preserves vertical wind shear and reveals many phenomena, such as hydrometeor transports and thermal advections, but it also fails to illuminate some mesoscale structure within MCSs. We adopted an environment-relative frame of reference, whereby the environmental wind relative to the MCS and MCV was removed. Few MCSs (e.g., Nachamkin and Cotton 2000) and no MCVs have been examined from this perspective. Results in the environ-

ment-relative frame of reference are especially valuable for comparison with fields of perturbations in three-dimensional wind within numerically simulated MCSs and MCVs.

The second point is the temporal variation in profiles of vertical velocity, divergence, and vorticity in the tropospheric column that contained the MCV. Because MCSs are long lived and mobile, and because dense observing networks occupy limited areas, detailed observations of MCVs over more than a few hours are rare. Fortunately, the MCS and MCV of 1 August 1996 matured and dissipated in the densest part of the NPN, so we were able to analyze 9 h of kinematical changes in the MCV. However, the data still fall short of fully describing the hourly changes in the life cycles of the system and vortex.

2. Data and methods

Observations are from the National Weather Service (NWS), remote sensors operated by NOAA, 1996's Enhanced Seasonal Observing Period (ESOP-96) of the Global Energy and Water Cycle Experiment's (GEWEX's) Continental-Scale International Project (GCIP), and the Oklahoma Climatological Survey's Oklahoma Mesonet (Brock et al. 1995).

a. Satellite and radar

Satellite data are from channels 1 (visible, 0.55–0.75 μm), 3 (water vapor, 6.50–7.00 μm), and 4 (infrared, 10.20–11.20 μm) of *Geostationary Operational Environmental Satellite-8* (*GOES-8*) and *GOES-9.*

Radar data are instantaneous composite reflectivity at an elevation angle of 0.5° with temporal and spatial intervals of 15 min and 2 km × 2 km. Each pixel for a specific point at a specific time is the highest reflectivity detected in a column by any radar. A 24-h animation of composite reflectivity provided the best overall, qualitative sense of the MCS's evolution. For more detailed analyses of the system and vortex we used the Weather Surveillance Radar-1988 Doppler (WSR-88D) Algorithm Testing and Display Program (WATADS 10.0) to examine level II data from WSR-88Ds at Oklahoma City, Oklahoma (KTLX), and Vance Air Force Base, Oklahoma (KVNX).

b. Observations near the ground

We inferred synoptic and mesoscale fronts near the ground primarily from our own manual analyses of temperature from observations in METAR, the international format for reporting surface weather, and from the Oklahoma Mesonet. When such analyses were insufficient, we referred to manually analyzed streamlines, radar reflectivity from WSR-88Ds, and satellite images from *GOES-8* and *GOES-9.* Some of our choices of mesoscale fronts were educated guesses, and we did not conduct detailed analyses of the fronts' sources.

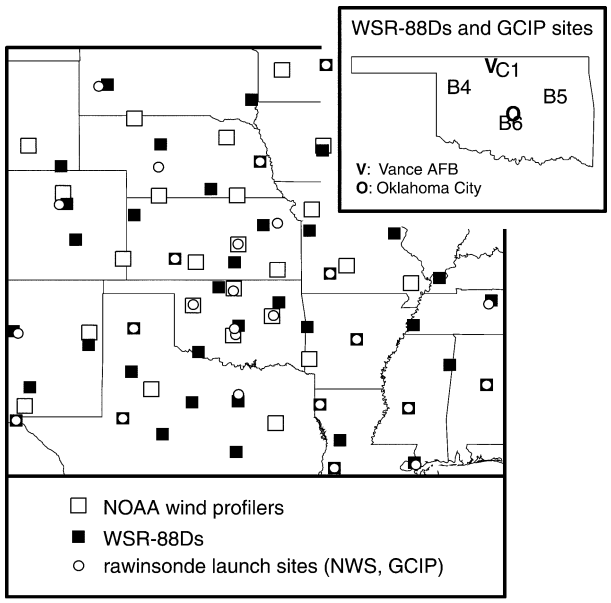

FIG. 1. Sites of observations above the ground. NOAA wind profilers are marked by large open squares, WSR-88Ds by small solid squares, and radiosonde launch sites of the NWS and GCIP ESOP-96 by small open circles. The inset map provides the locations of specific WSR-88D and GCIP sites.

c. Soundings

Tropospheric soundings are from the NPN (Weber et al. 1993; Barth et al. 1994), radiosondes launched semidaily by the NWS, and radiosondes launched every 3 h from four sites in Oklahoma during ESOP-96 of GCIP (Fig. 1).

We analyzed hourly data from the NPN taken from 0.5 to 16.25 km above ground level (AGL), excluding data that failed NOAA's checks for temporal and spatial continuity (Weber et al. 1993) and their check for contamination by migrating birds (Barth 1998, personal communication). We inspected all soundings for gross errors, which we removed, and linearly interpolated in the voids.

From 0900 to 1800 UTC on 1 August, what we call the *period of detailed analysis,* 12% of soundings were missing at the NPN sites closest to the MCS, and 13% were missing at the seven most densely spaced sites (Fig. 1). Only at 1800 UTC was a GCIP sounding available to be substituted for a missing NPN sounding.

For thermodynamic soundings, convective available potential temperature (CAPE) and convective inhibition (CIN) were calculated for a thoroughly mixed boundary layer 10 hPa deep for morning soundings, which displayed nocturnal inversions, and 100 hPa deep for afternoon soundings. Because proximate soundings were taken as much as 2 h 15 min before the MCS arrived

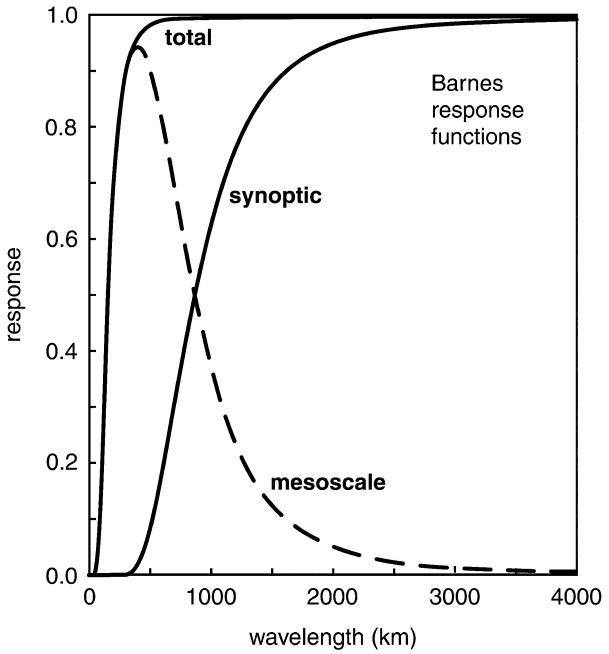

FIG. 2. Response functions for the Barnes analyses.

at a site, we adjusted the mean temperature in the lowest 10 hPa of soundings in order to better approximate conditions just prior to the system's arrival. Adjustments, which ranged from $-0.2°$ to $+1.9°$C, were made to match the changes in 5-min temperature at the Oklahoma Mesonet station closest to where each sounding was taken.

d. Objective analyses and bandpass filtering

To produce gridded fields of total wind, $\mathbf{u}(u, v, w)$, we used a two-pass Barnes analysis (Barnes 1973; Koch et al. 1983) on data from the NPN. Grid points were 75 km apart, the cutoff radius was 750 km, and the response function was chosen to capture 90% of the signal of phenomena with wavelengths of 300 km, which is twice the average distance between profilers in the densest part of the NPN (*total* curve in Fig. 2). Less than 10% of the signal of phenomena with wavelengths shorter than 85 km was captured, so virtually no coherent convective signal exists in the analyzed data.

To partially isolate the mesoscale kinematics of the MCS from the synoptic kinematics, we employed a second Barnes analysis. Together with the first, it acted as a bandpass filter (Maddox 1980). The synoptic background wind, $\tilde{\mathbf{u}}(\tilde{u}, \tilde{v}, \tilde{w})$, was approximated with data filtered to include 90% and 0.09% of the signals of phenomena with wavelengths of 1600 km and 300 km, respectively (*synoptic* curve in Fig. 2). This is the same filtration Maddox (1980) used for synoptic features. The mesoscale perturbation in wind, $\hat{\mathbf{u}}(\hat{u}, \hat{v}, \hat{w})$, was approximated by subtracting the synoptic background wind from the total wind (*mesoscale* curve in Fig. 2).

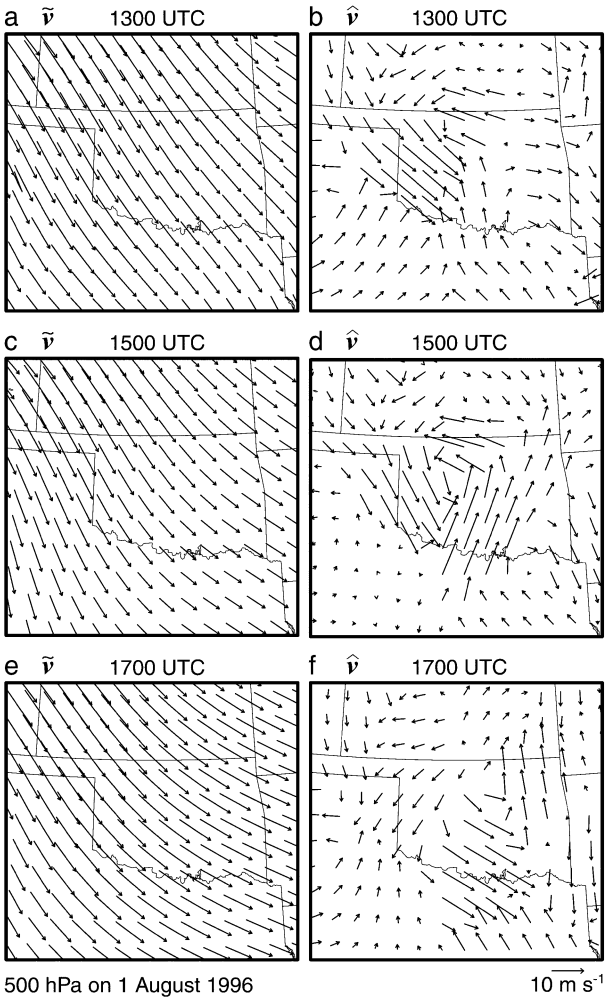

FIG. 3. Winds at 500 hPa, 1 Aug 1996. The rows from top to bottom are for 1300, 1500, and 1700 UTC; the columns from left to right are the synoptic background wind and the mesoscale perturbation in wind.

In summary, $\mathbf{u}(u, v, w) = \tilde{\mathbf{u}}(\tilde{u}, \tilde{v}, \tilde{w}) + \hat{\mathbf{u}}(\hat{u}, \hat{v}, \hat{w})$. Sometimes we refer to the components here simply as the *synoptic wind* and the *mesoscale wind*. Figure 3 shows examples of them and demonstrates that the technique capably resolved the MCV of 1 August as it moved southeastward across Oklahoma.

The right column of panels in Fig. 3 may give the impression of discontinuities in the mesoscale wind, discontinuities that would produce unrealistic derivatives. That impression seems to be an artifact of the eyes' interpretation of vectors, though, because vorticity (Fig. 4) and divergence (not shown) of the mesoscale wind are acceptably smooth.

The bandpass filter did not completely isolate the mesoscale and synoptic winds from each other, especially at scales near where the two response curves cross (Fig. 2). According to virtually all systems of scale classification, the mesoscale at midlatitudes includes phenomena with characteristic lengths in the hundreds of ki-

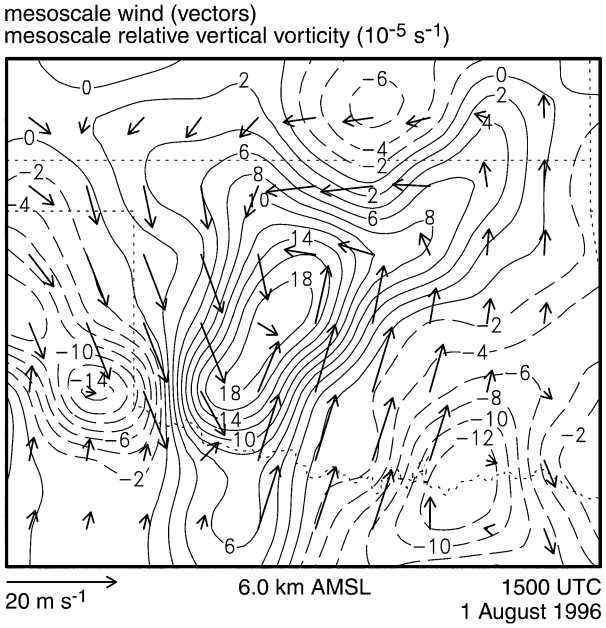

FIG. 4. Mesoscale wind (m s^{-1}) and vorticity (10^{-5} s^{-1}) at 6.0 km AMSL at 1500 UTC 1 Aug 1996.

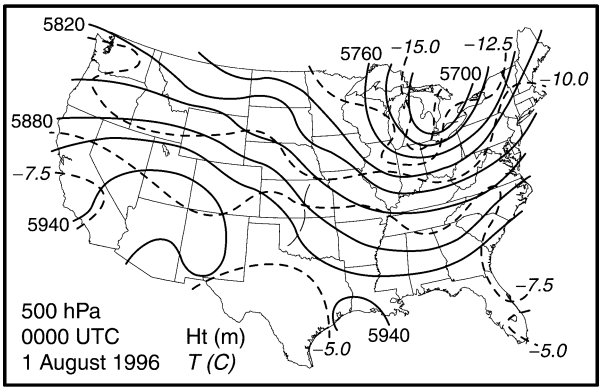

FIG. 5. Height (m AMSL, solid) and temperature (°C, dashed) at 500 hPa at 0000 UTC 1 Aug 1996. The thin line with long dashes marks the axis of a short-wave trough.

lometers (e.g., Ligda 1951; Orlanski 1975; Fujita 1981; Emanuel 1983), so what we call here the *synoptic background wind* does contain some mesoscale signal. However, the wavelengths of the MCS and MCV of 1 August 1996 were near the peak of the mesoscale response function, ~400 km, where the synoptic part of the filter was quite insensitive.

e. Divergence and vorticity

We calculated divergence and vorticity in two ways. Results in this paper are from centered finite differences of objectively analyzed fields of u and v components of wind. This method can produce derivatives corrupted by noise (Schaefer and Doswell 1979), so we tested it against line integrals of tangential and normal components of wind calculated around the perimeters of triangles whose vertices were the profilers (Ceselski and Sapp 1975). The two methods produced comfortingly similar results.

f. Vertical velocity

Vertical velocity is from the kinematical method with a linear correction to density-weighted divergence (O'Brien 1970), for which we set $w = 0$ at 750 m above the tropopause and $w = 0$ at 500 m AGL. The upper condition is based on work by Johnson et al. (1990), who showed that vertical velocity above the stratiform region of the MCS of 10–11 June 1985 was close to zero 1 km above the tropopause. The lower condition was a pragmatic choice; surface data at the NPN sites were unavailable, and Brandes (1990) and others showed that magnitudes of mesoscale vertical motions near 500 m AGL in the presence of MCSs are only 0–5×10^{-2} m s^{-1}.

g. Spatial and temporal extent of the MCV

We diagnosed the center of the MCV to be at the center of the observable cyclonic motion in composite radar reflectivity and considered the MCV to have formed when a cyclonic circulation appeared and to have dissipated when that cyclonic circulation disappeared. Proximate radar echoes were present before, during, and after the MCV's lifetime, so it is quite unlikely that the MCV existed long before or after it was detectable with radar, but with other MCVs this is often not the case. Methods of locating the MCV based on kinematical and thermodynamical data proved too sensitive to the coarseness of observations, producing closed streamlines and maxima in vorticity that unrealistically jumped hundreds of kilometers from one time to the next. Methods based on satellite data were impossible due to cirri above the swirl of clouds in the middle troposphere.

Because of the coarseness of the kinematical data, it was not possible to do more than estimate the size of the MCV at certain times when the vortex seemed best observed. The radius of maximum wind was approximately 0.75°–1.50° latitude (83–167 km). The rotating cloud shield extended beyond the radius of maximum wind—which is common (e.g., Fritsch et al. 1994)—to a radius of approximately 2.0° latitude (222 km). Some have estimated the perimeter of MCVs with contours of vorticity (e.g., Brandes and Ziegler 1993). The weakness in this method is that horizontal shear near MCSs often contributes large vorticity, which can elongate contours or displace even quasicircular contours well away from the center of an MCV's rotation.

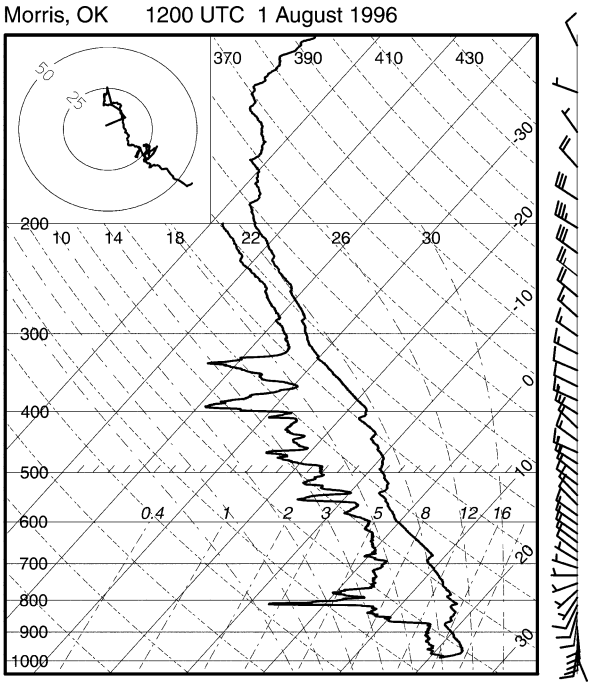

FIG. 6. GCIP sounding for Morris, OK (B5 in Fig. 1), at 1200 UTC 1 Aug 1996. Half and full wind barbs respectively represent 5 and 10 m s^{-1}. CAPE was 704 J kg^{-1} and CIN was 133 J kg^{-1}. This sounding is representative of those taken ahead of the MCS early on 1 Aug.

h. Averaging and construction of schematic cross sections

Although the NPN provided a much more resolved dataset than would have been available from operationally launched radiosondes alone, missing data still made it impossible to construct detailed analyses at every individual hour, especially late in the lives of the MCS and MCV. We mitigated this problem in two ways. First, we examined spatial and temporal averages of vertical velocity, divergence, and vorticity in the stratiform region. The averages were usually over 3 h and a 2° × 2° area centered on the MCV. Second, we scrutinized vertical and horizontal cross sections of wind only for times at which the most data were available, and present cross sections that are schematic representations of data at those times. (The analyses of perturbation wind shown in Figs. 3b, 3d, and 3f are examples of sources for the schemata.) This allows depiction of features that appear in various datasets, sometimes at various times, in a way we believe best represents the kinematics of the MCS and MCV.

3. Overview of synoptic and mesoscale environments

The MCS formed at 0430 UTC on 1 August 1996 and had completely dissipated by 0315 UTC on 2 August. The MCS's environment was not different in any important way from the environments of other observed MCSs that generated MCVs (e.g., Bartels and Maddox 1991; Trier et al. 2000b).

a. Conditions above the ground

The MCS originated in northwesterly wind upstream of conditionally unstable air. Vertical shear was weak to moderate (generally less than 3×10^{-3} s^{-1} from 2 to 6 km, for example). The northwesterlies were a result of a ridge centered over the Colorado Plateau and a trough centered over the Great Lakes (Fig. 5). Within the northwesterlies was a short-wave trough in the lower and middle troposphere (long-dashed line over Kansas and Oklahoma in Fig. 5). Vorticity advection at 500 hPa was weak to nonexistent (not shown).

Four soundings taken from 0900 to 1200 UTC ahead of the MCS display a shallow nocturnal inversion surmounted by layers of weak conditional instability from the lower to the upper troposphere. A warm, dry layer was centered at an average of 770 hPa. (Figure 6 is an example of the four soundings.) Values of CAPE and CIN are given in Table 1. The values cover a considerable range. If the vigor of the system around 1200 UTC is an indication, the higher values of CAPE and lower values of CIN are likely the more representative.

Because the last of these four soundings ahead of the MCS was taken at 1200 UTC, they almost certainly do not represent the environment that the declining and dissipating MCS encountered later in the day. The sounding taken at 0000 UTC on 2 August at Shreveport, Louisiana, approximately 200 km southeast of where the MCS dissipated, registered a mixed layer nearly 1 km deep, CAPE of 2513 J kg^{-1}, and CIN of 6 J kg^{-1}.

TABLE 1. Environmental CAPE and CIN ahead of the MCS. Values labeled *observed* are calculated directly from each sounding. Values labeled *forecast* are calculated after the mean temperature in the lowest 10-hPa of each sounding was raised or lowered based on observations from nearby OK Mesonet sites just prior to arrival of the MCS.

GCIP sounding station	Time of sounding (UTC)	Hours prior to MCS	Observed		Forecast	
			CAPE (J kg^{-1})	CIN (J kg^{-1})	CAPE (J kg^{-1})	CIN (J kg^{-1})
B4	0900	1.00	1483	91	1317	104
B5	1200	2.25	704	133	2116	2
B6	1200	1.00	500	166	636	135
C1	0900	1.50	321	305	466	263

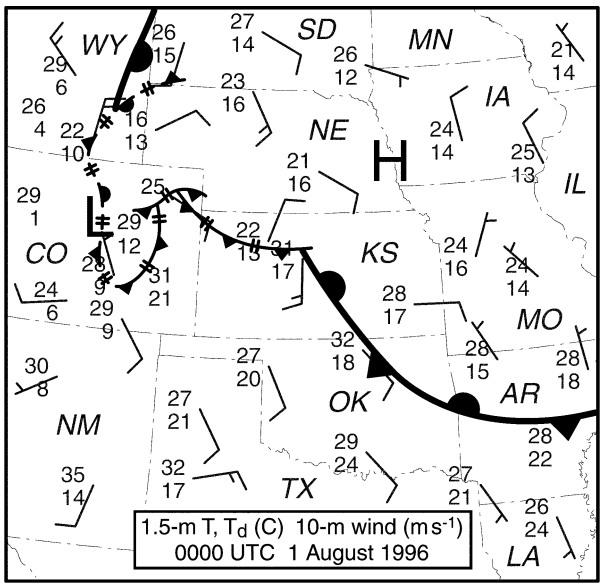

FIG. 7. Synoptic and mesoscale fronts at 0000 UTC 1 Aug 1996. Station models display temperature and dewpoint (both °C), and wind, for which full and half barbs respectively represent 2.5 and 5.0 m s^{-1}. An absent vector indicates a missing observation, not calm conditions.

We speculate that these values approximately represent the environment of the MCS during the afternoon of 1 August.

The average altitude of the tropopause near the MCS was 15.73 km above mean sea level (AMSL) (116 hPa) and the average altitude of 0°C was 4.48 km (596 hPa). A weak to moderate southerly low-level jet (Whiteman et al. 1997) appeared between 100 and 500 m AGL in the vicinity of the MCS after nightfall (not shown). At the jet's altitude, gradients in temperature and moisture were small, so advections were weak.

These tropospheric conditions were similar to those in environments of other MCSs that generated MCVs. Bartels and Maddox (1991) showed that 29% of MCVs in the population they studied formed in northwesterly wind between a ridge and trough at 500 hPa, and weak vorticity advection and low-level jets were common. Bartels and Maddox (1991) and Trier et al. (2000b) noted high CAPE ahead of many of the MCVs in their studies. The latter found that CAPE averaged 1895 J kg^{-1} among MCVs that fostered a secondary MCS. The MCV of 1 August 1996 did foster secondary cumulonimbi, but not in the form of an MCS.

b. Conditions near the ground

A synoptic stationary front extended southward through the western High Plains, then southeastward across the Great Plains (Fig. 7). At 0000 UTC on 1 August, three mesoscale fronts disrupted and modified the synoptic front in Wyoming, Colorado, and Kansas. These fronts appeared to be the leading edges of outflow from unorganized clusters of cumulonimbi, but data were inconclusive. (Fronts were determined from observations more dense than those reproduced in Fig. 7.)

Trier et al. (2000b) found that over half the MCVs in the central United States during 1998 were generated by MCSs that formed near synoptic surface fronts. Most of these MCSs originated on the cold side of east–west, quasi-stationary fronts like the one in Fig. 7. After it formed, the MCS of 1 August 1996 soon moved south of the synoptic front. Although the MCS's outflow effectively kept the system on the cool side of a mesoscale front, deep towers in the convective line were fed by warm environmental air from the south.

4. Life cycles of the MCS and MCV

The MCS studied herein was the largest, but not the only, organized system of cumulonimbi in the central United States on 1 August 1996; another, smaller vortical system formed in South Dakota and crossed Nebraska (the states, but not the smaller system, are shown in Fig. 7). At various stages, the larger MCS (and, henceforth, the only one to which we will refer) exhibited many classic characteristics of MCSs that generate

TABLE 2. Stages of the MCS of 1 Aug 1996 diagnosed from composite reflectivity.

Stage	Time (UTC)	Characteristics
Prelude	0215–0330	Scattered cumulonimbi form prior to the MCS
Formation	0345–0415	Three clusters of cumulonimbi merge
	0430–0530	Indistinguishable clusters become the incipient MCS
Development	0545–0700	MCS is quasi-symmetric with a linear convective line of reflectivity ≥45 dB*Z*
	0715–0845	MCS becomes asymmetric when the first of two notches develops at the back edge of the stratiform region and the convective line bows into the shape of an S
Maturity	0900–1130	Northern part of the *S*-shaped convective line becomes fractured; otherwise the MCS changes little
Decline	1145–1530	MCS weakens as a second notch develops at the back edge of the stratiform region; the convective line breaks apart; the northern side of the stratiform region takes on the appearance of a hammer head
Dissipation	1545–0315	Remnants of the MCS take the form of spiral bands that slowly dissipate; spotty new cumulonimbi grow among old cumulonimbi

MCVs (Table 2 and Fig. 8). Early symmetry gave way to asymmetry as the MCS matured. (This symmetry, along-line symmetry, is about the system's vector of motion, imagined to be drawn through the center of the convective line.) This exemplifies conclusions by Skamarock et al. (1994), Loehrer and Johnson (1995), and others that *symmetric* and *asymmetric* are adjectives that should be applied to stages in some MCSs, not to MCSs as a whole.

a. Formation

The MCS formed with the merger of three clusters of cumulonimbi between 0345 and 0415 UTC on 1 August. The first cluster, A in Fig. 8a, emerged from a large mass of cumulonimbi in the panhandle of Nebraska. The second cluster, B, appeared to form along the short mesoscale front in the northeastern corner of Colorado (Fig. 7). The third cluster, C, formed along the mesoscale front in northwestern Kansas. Between 0430 and 0530 UTC the three clusters became indistinguishable; they were the incipient MCS.

b. Development

The MCS spent 1 h 15 min in approximate symmetry about its vector of motion, beginning at 0545 UTC when a convective line roughly 275 km long produced contiguous reflectivity of 45 dB*Z* (Fig. 8b). The MCS's symmetry was approximate in that reflectivity from cumulonimbi was highest at the center of the convective line, as in the schema of a symmetric system by Houze et al. (1990), but reflectivity in the stratiform region was highest on the MCS's left, as in their schema of an asymmetric system. (*Right* and *left* are from the perspective of the advancing MCS; its left side was generally to the northeast and its right side was generally to the southwest.) Late in the symmetric stage of the system there were signs of the MCV in Doppler wind from KVNX, which is consistent with the possibility that heating in the stratiform region of the MCS generated the vortex.

Following the symmetric stage, the convective line remained vigorous and the MCS became highly asymmetric. Its transition to along-line asymmetry began at 0715 UTC when a notch developed at the back edge of the stratiform precipitation (N1 in Figs. 8c,d) and the convective line started to bow into the shape of an *S* (Figs. 8c,d). Notch N1 initially appeared to be the lingering signature of a gap where clusters A and B merged to form the incipient MCS (cf. Figs. 8a and 8c). However, the notch persisted through later stages of the MCS (Fig. 8d). Smull and Houze (1987) found a similar coincidence between notching of a stratiform region and bowing of a convective line within the MCS of 22 May 1976. They hypothesized that strong inflow from behind the MCS in the middle troposphere dried the stratiform region, descended, and overtook the convective line, accelerating it forward. This same sequence of events most likely explains the asymmetric deformation of the MCS of 1 August 1996, although sparse coverage of the NPN prevented us from determining this conclusively.

During the hour after the initial bowing at 0715 UTC, the stratiform region became dramatically enhanced; reflectivity in active, embedded cumulonimbi exceeded 50 dB*Z*. As rainfall rate increased and the stratiform region expanded, a small cluster of heavily precipitating clouds overtook the existing stratiform region from behind and merged with it (not shown). It was at the time of the deformation of the convective line into the *S* shape and of this merger that the MCS became most asymmetric (Fig. 8d).

c. Maturity

From 0900 to 1130 UTC the MCS changed little, apart from some fracturing of the northern part of the convective line (the northern, concave of the two curves that composed the *S* shape), which left only a single, convex arc of cumulonimbi at the leading edge of the MCS. In an approach similar to that of Hilgendorf and Johnson (1998), we designated this period as the mature stage because of the MCS's minimal change and because the system comprised the main reflectivity features that characterize asymmetric MCSs of this kind: a bowed convective line followed by stratiform precipitation—some of which includes enhanced radar returns—on the system's left side.

d. Decline

At 1100 UTC the right half of the MCS overtook in western Oklahoma a broad, seemingly unorganized north–south band of cumulonimbi (Fig. 8e). The unorganized band effectively became the right side of the MCS's convective line. At 1145 UTC reflectivity within the convective line started to decrease from over 50 dB*Z* along most of its right half to only 40 dB*Z* in isolated patches by 1345 UTC (not shown).

Between 1145 and 1530 UTC a second notch formed at the back of the MCS (N2 in Figs. 8f and 8g). As notch N2 advanced deeply and cyclonically into the left part of the stratiform region, reflectivity on the MCS's far left took on the shape of a hammer head (Fig. 8g), and the stratiform region broke into spiral bands of clouds that continued to rain with reflectivity between 15 and 35 dB*Z*. This second notch, like the first, was almost certainly symptomatic of dry air intruding at the back of the MCS. Notches and spiral bands within stratiform regions that contain MCVs are common (e.g., Smull and Houze 1987; Fritsch et al. 1994), but they do not accompany every MCV (e.g., Chong and Bousquet 1999), nor are they infallible signs of MCVs (e.g., Fortune et al. 1992).

At no time did any of our data expose an anticyclonic

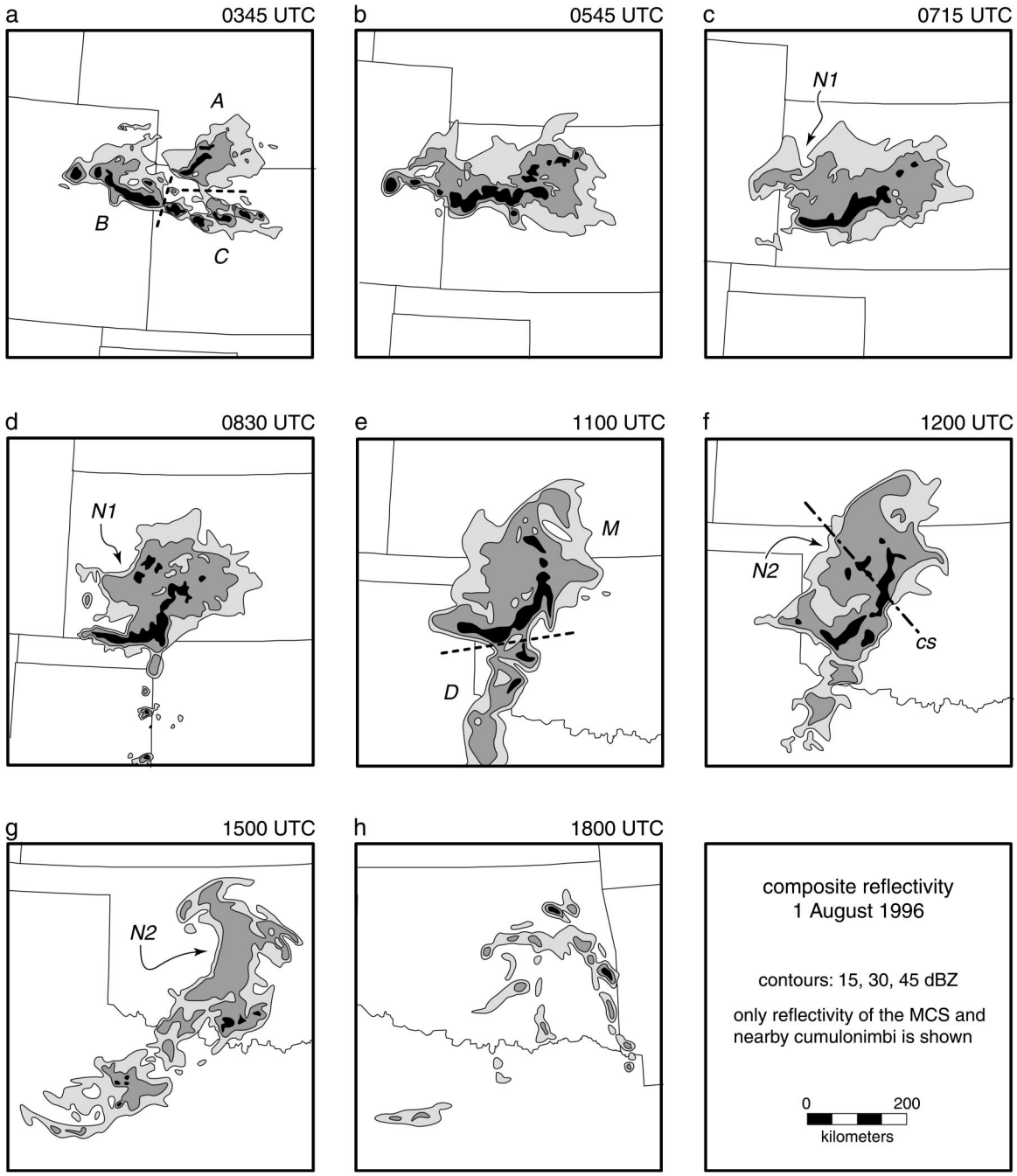

FIG. 8. Schemata of composite base-scan radar reflectivity on 1 Aug 1996. Times are (a) 0345, (b) 0545, (c) 0715, (d) 0830, (e) 1100, (f) 1200, (g) 1500, and (h) 1800 UTC. Contours are at 15, 30, and 45 dBZ. Only reflectivity due to the MCS and nearby cumulonimbi is shown. Clusters that merged to form the MCS are separated by dashed lines and marked by A, B, and C. A band of cumulonimbi overtaken by the MCS, M, is marked by D; the two are separated by a dashed line. Notches are marked by N1 and N2. The location of the cross section in Fig. 13 is marked by cs.

vortex on the right side of the MCS of 1 August 1996, although vorticity there was often strongly negative from horizontal shear. Anticyclonic vortices are sometimes paired with cyclonic vortices in MCSs (e.g., Scott and Rutledge 1995), although the former tend to be smaller, weaker, and more short lived.

e. Dissipation

In the lengthy final stage of the MCS, from 1545 UTC on 1 August through 0315 UTC on 2 August, the spiral bands slowly dissipated, and spotty new cumulonimbi grew in the remnants of the bands (Fig. 8h). Clusters

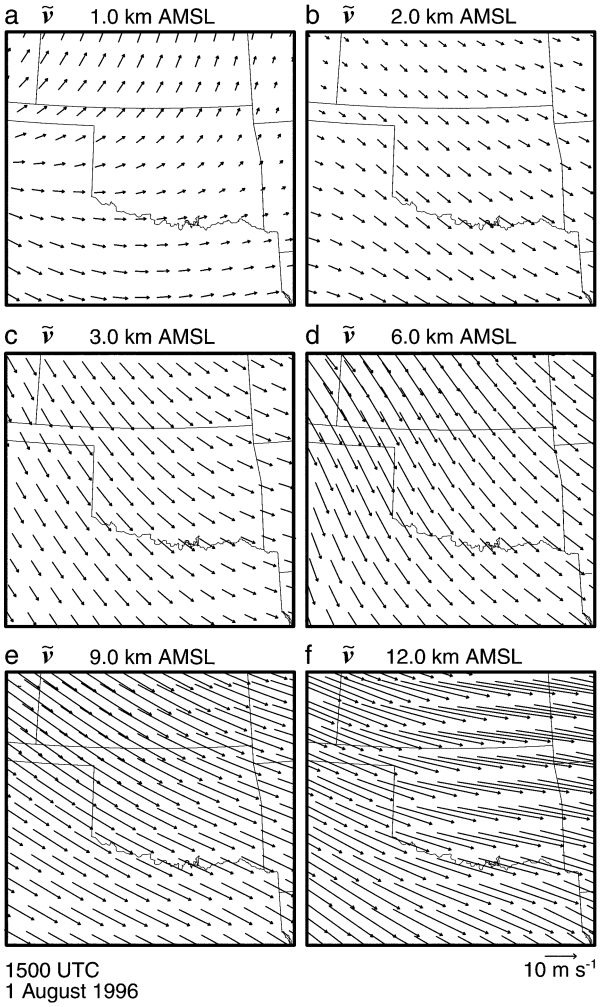

FIG. 9. Synoptic wind at 1500 UTC 1 Aug 1996. Altitudes are (a) 1.0, (b) 2.0, (c) 3.0, (d) 6.0, (e) 9.0, and (f) 12.0 km AMSL.

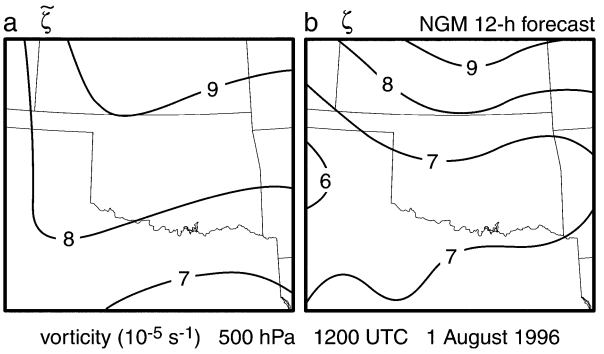

FIG. 10. Vorticity at 500 hPa at 1200 UTC 1 Aug 1996. The panels show (a) vorticity of the synoptic background wind and (b) the NGM's 12-h forecast of vorticity from the model run initialized at 0000 UTC 1 Aug 1996.

of cumulonimbi that were traced to these dissipating bands persisted through 2 August in Arkansas, Louisiana, and Mississippi, but no sustained mesoscale vortical patterns were visible in the clusters, nor did the clusters display in the radar data any mesoscale organization.

5. Wind

Only the densest part of the NPN provided data that were sufficiently resolved to diagnose the mesoscale kinematical imprint of the MCS on its environment. This forced us to restrict the analyses to between 0900 and 1800 UTC, which encompassed the MCS's asymmetric period from maturity through dissipation (Table 2).

a. Synoptic background wind

The synoptic background wind over the parts of Kansas and Oklahoma in the warm sector of the synoptic frontal system veered from southeasterly near the ground (Fig. 7) to westerly between 1.0 and 2.0 km AMSL and northwesterly or west-northwesterly above that (Fig. 9). Synoptic wind was northwesterly in the middle troposphere where the MCV formed (Figs. 9c,d).

At 1200 UTC, absolute vorticity at 500 hPa was between 6 and 10 $\times$ 10^{-5} m s^{-1} (Fig. 10a), due partly to a short-wave trough (Fig. 5). Vorticity in the synoptic background flow was somewhat similar to vorticity in the 12-h forecast by the Nested Grid Model (NGM) initialized at 0000 UTC on 1 August (cf. Figs. 10a and 10b). In particular, both fields contained a minimum in vorticity through central Kansas, western Oklahoma, and the Texas Panhandle. The NGM did, however, produce an unmatched east–west minimum in vorticity through southern Oklahoma, and the highest gradients in vorticity exceeded those in the observed synoptic wind. This is not surprising because the NGM resolved smaller phenomena than were retained in the observations after the synoptic bandpass filter was applied.

The extent to which Figs. 10a and 10b are similar suggests that synoptic vorticity over Kansas and Oklahoma was largely due to numerically predicted phenomena. The MCS did not exist at 0000 UTC, so it was not represented in data used to initialize the NGM, nor was the MCS predicted by the NGM, although the model did forecast widespread rain. Similarity between the forecast field that did not include the MCS and what we have calculated to be synoptic background wind substantiates our method of discriminating between the convective system and its environment.

b. Mesoscale perturbation in wind

Observations from the NPN at 1200 UTC exemplify the mesoscale wind during the MCS's maturity (Fig. 11), and observations from 3 h later exemplify the mesoscale wind during the MCV's maturity (Fig. 12). However, because no instrument platform was able to observe completely all of the important mesoscale struc-

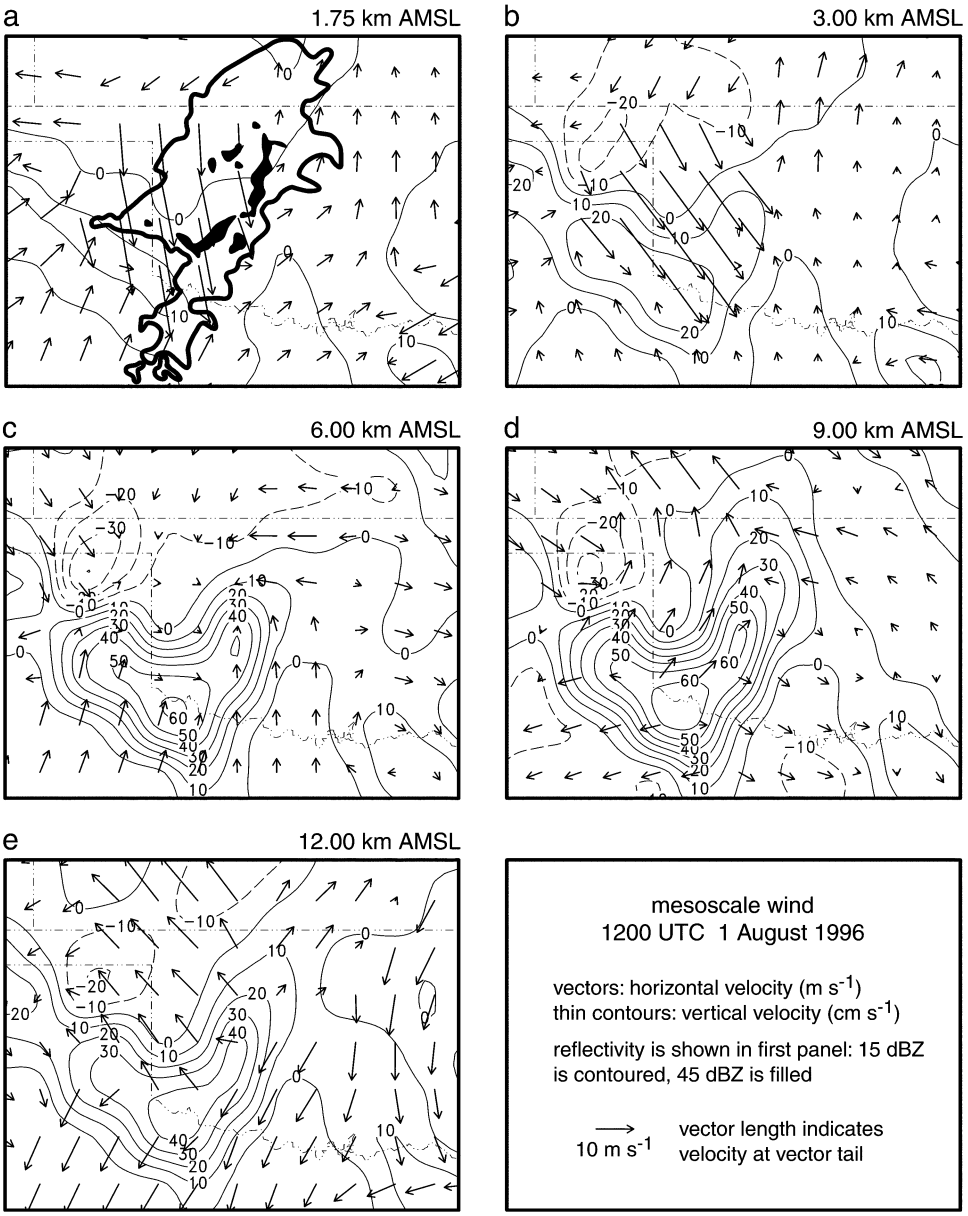

FIG. 11. Three components of the mesoscale wind at 1200 UTC 1 Aug 1996. The altitudes are (a) 1.75, (b) 3.00, (c) 6.00, (d) 9.00, and (e) 12.00 km AMSL. Vectors represent horizontal velocity, and vertical velocity is contoured in thin lines every 10 cm s^{-1}. In (a), reflectivity of 15 dBZ is contoured in the thick line and >45 dBZ is filled.

ture of the system and vortex at every hour, we have chosen to summarize data from multiple hours and multiple platforms in the form of schemata (Figs. 13 and 14). The two most consistent problems with data from the NPN at individual hours were, first, that the main mesoscale features in the wind field were often mislocated even when the features were distinctly apparent, and, second, that a few entirely erroneous features were nearly always present. The former can be explained by the distance between wind profilers. An example of the latter is the north–south couplet of descent and ascent above 6 km AMSL in the Texas Panhandle that appears in Figs. 11 and 12.

During the MCS's maturity, the mesoscale perturbation in wind included a mesoscale updraft and downdraft, divergent outflow in the lower troposphere, divergent outflow in the upper troposphere, and an MCV centered in the middle troposphere (Figs. 11–14). Apart from the MCV, these are the four primary mesoscale circulations portrayed in other depictions of wind within MCSs (e.g., Zipser 1977; Smull and Houze 1987; Johnson et al. 1990). Because these circulations appear in

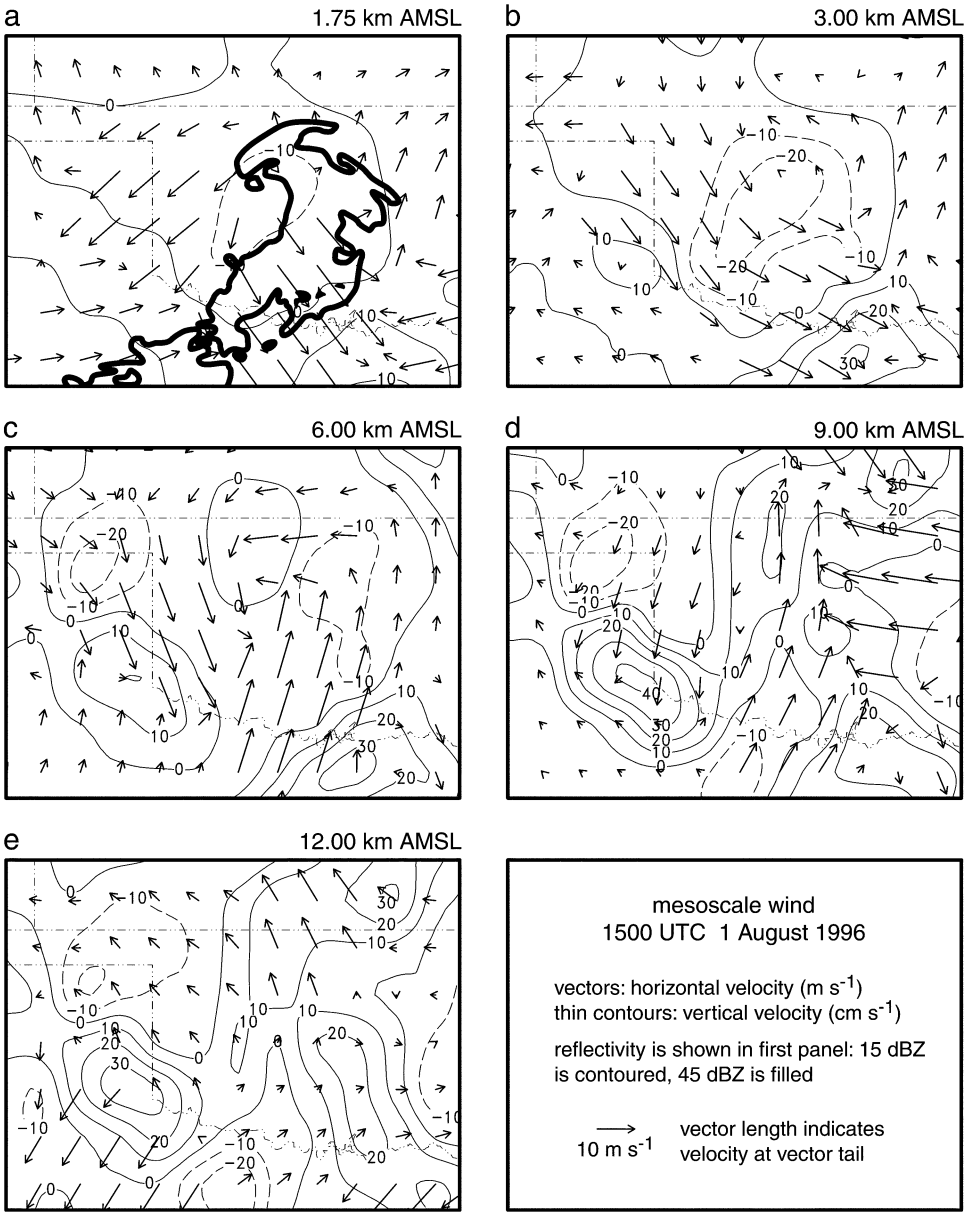

FIG. 12. Three components of the mesoscale wind at 1500 UTC 1 Aug 1996. The altitudes are (a) 1.75, (b) 3.00, (c) 6.00, (d) 9.00, and (e) 12.00 km AMSL. Vectors represent horizontal velocity, and vertical velocity is contoured in thin lines every 10 cm s^{-1}. In (a), reflectivity of 15 dBZ is contoured in the thick line and >45 dBZ is filled.

the mesoscale perturbation in wind, we conclude they were internal and fundamental to the MCS of 1 August 1996; they were not merely *apparent* circulations that resulted from a ground-based frame of reference or from the superposition of the MCS flow, the environmental flow, and the translational motion of the MCS relative to the environmental flow. Others have concluded the same about different MCSs (e.g., Smull and Houze 1987).

A mesoscale rear inflow jet entered the MCS at the back edge of the stratiform region, primarily below 9 km AMSL (Figs. 11a–d, 12a–d, 13a, and 14a,b), in the middle part of the MCS, away from its left and right ends. This inflow jet was the rear part of the mesoscale downdraft. Air in the downdraft flowed through the lower part of the anvil and beneath the anvil's base, then descended beneath a mesoscale updraft (Fig. 13a). The mesoscale downdraft was strongest between 2 and 6 km AMSL (Figs. 11b, 12b, and 13a). (In Fig. 13, ground level is approximately 0.3 km AMSL.) The rear inflow jet is apparently one reason that rain-free air advanced into the stratiform region, forming the second notch as

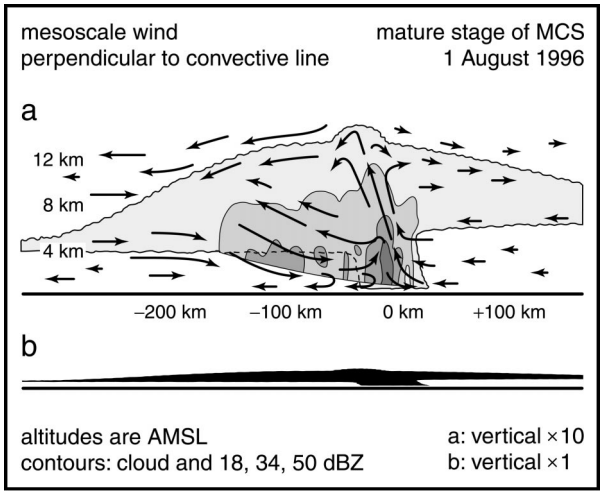

FIG. 13. Schematic cross section of reflectivity and the cross-line component of the mesoscale perturbation in wind. Arrows are a hybrid of vectors and streamlines, and their lengths roughly indicate relative wind speed of consistently observed flows along various locations in the MCS as determined from the NPN at 1200 UTC and from cross sections of WSR-88D Doppler velocity from KTLX from 1233 to 1320 UTC. Contours are cloud edge and reflectivity of 18, 35, and 50 dBZ. Reflectivity is at 1233 UTC along the line shown in Fig. 8f. The bottom edge of the reflectivity cross section is due to the lower limit of the lowest radar scan. Cloud top is from a *GOES-8* IR image at 1215 UTC along the same cross section; cloud bottom is estimated from GCIP soundings at 1200 UTC and from other studies of MCSs. Height is exaggerated by a factor of 10 in (a); (b) an unexaggerated silhouette.

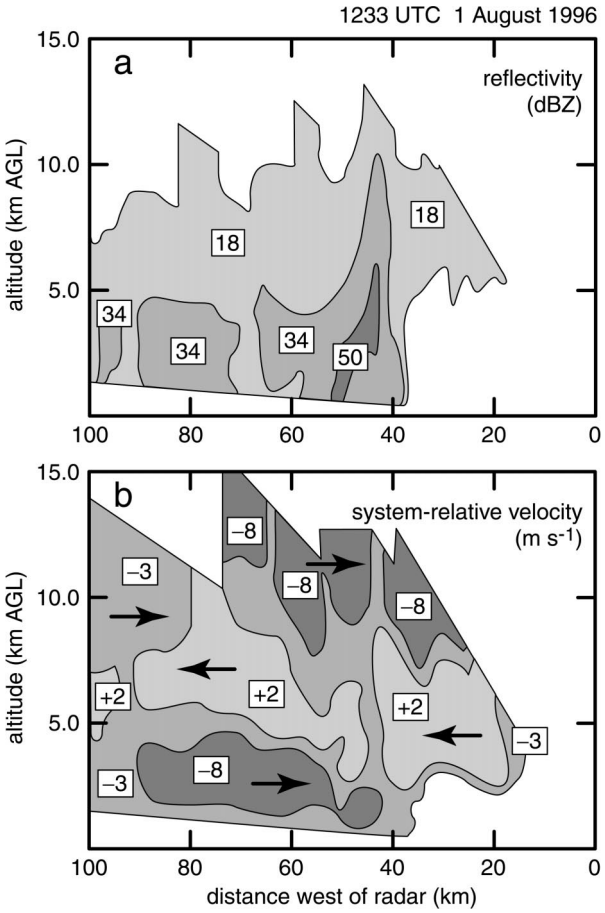

FIG. 15. Cross section of level II data through the middle of the mature MCS at 1233 UTC 1 Aug 1996. Panels show (a) regions of reflectivity enclosed by contours of 18, 34, and 50 dBZ; and (b) regions of system-relative radial wind enclosed by contours of 8 and 3 m s^{-1} toward the radar (westerlies), and 2 m s^{-1} away from the radar (easterlies). The section was taken along the 270° radian.

the MCS declined. There is evidence that in some places the mesoscale downdraft continued through the convective line and emerged in front of the leading cumulonimbi. For example, in the middle of the mature MCS at 1250 UTC, a rear-to-front (RTF) flow (both in a storm-relative and an environment-relative framework) in the lower troposphere extended farther eastward than the high reflectivity of the convective line (Fig. 15).

A mesoscale updraft lay above the mesoscale downdraft (Figs. 11c–e, 12d,e, and 13a). Level II Doppler velocity from KTLX shows that in cross section the surfaces of highest wind speeds in both drafts were concave, as seen from above, between the convective line and the enhanced reflectivity in the stratiform region. The mesoscale updraft originated at about 5 km AMSL along the back edge of updrafts in the convective line. The mesoscale updraft was at times distinct to an alti-

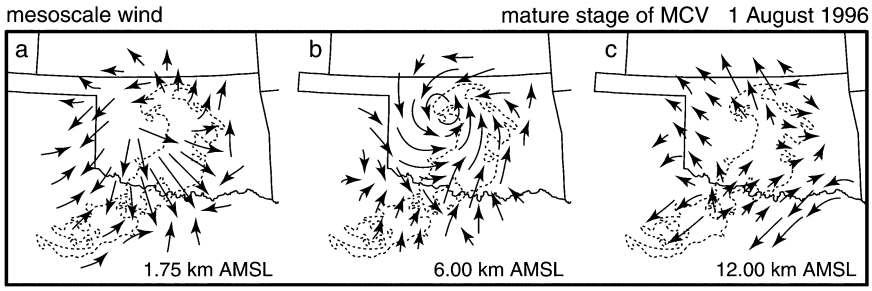

FIG. 14. Schemata of horizontal mesoscale perturbation in wind at 1500 UTC 1 Aug 1996. Altitudes are (a) 1.75, (b) 6.00, and (c) 12.00 km AMSL. Arrows are a hybrid of vectors and streamlines, and their lengths roughly indicate relative wind speed. The contour of 15 dBZ reflectivity within the MCS is dashed.

tude of more than 10 km AMSL farther than 150 km behind the convective line. The fact that data from the NPN shows that flow within the updraft gradually veered as it ascended and advanced rearward through the stratiform region (at the northern end of the MCS in Figs. 12c–e and 14) suggests that planetary vorticity turned the mesoscale updraft to the right as it ascended, in the manner described by Skamarock et al. (1994) and Scott and Rutledge (1995). Locally high wind speed in the divergent southeasterly flow on the northern side of the MCS at 12 km AMSL—where we will later show upper-tropospheric divergence above the MCV was maximized—appeared to be part of the veering, ascending mesoscale updraft as it exited the cloud and precipitation of the MCS (Figs. 12e and 14c). These altitudes are above echoes returned to the WSR-88D at KTLX, so this speculation cannot be confirmed with more resolved data. Air in slanted updrafts of the convective line decelerated when beyond its level of buoyant equilibrium, which also contributed to divergent outflow in the upper troposphere (Fig. 13a).

At 1.75 km AMSL—where we will later show lower-tropospheric divergence in the MCV was maximized—diverging air beneath and behind the precipitation of the stratiform region converged with air in a ring around the perimeter of the precipitation of the MCS. Convergence in this ring was greatest near the southeastern and southern perimeter of the MCS's reflectivity (Figs. 11a, 12a, and 14a). Numerical simulations by Skamarock et al. (1994) demonstrated that such locally maximized convergence on the right side of a convective line characterizes MCSs that mature where planetary vorticity is large. Divergent northwesterly wind at 1.75 km AMSL behind the precipitation of the stratiform region was likely the terminus of the mesoscale downdraft.

Air descended broadly and weakly along the top of front-to-rear (FTR) flow behind the convective line (Figs. 11e and 13a). Johnson et al. (1990) noted broad descent at a similar altitude in the MCS of 10–11 June 1985. In that MCS, descent was in storm-relative flow within isentropic layers that sloped downward away from the convective line along the top of the stratiform anvil. That explanation is consistent with data from the MCS of 1 August 1996.

As the caption to Fig. 13 states, our diagnosis of cloud top is based on infrared data from *GOES-8*. The slope of the cloud top is steeper than the slopes of clouds in schemata by Houze et al. (1989), Biggerstaff and Houze (1991), and others, so we scrutinized channels 1 and 3 from *GOES-8* and checked soundings to the west of the MCS to determine whether thin anvil in the upper troposphere may have escaped detection in the infrared channel. We found no evidence that indicated our depiction of cloud top is wrong. One possible explanation for lack of high clouds well behind the MCS is that a region of dry air in the upper troposphere lay immediately to the west of the center of the MCS cloud shield (not shown).

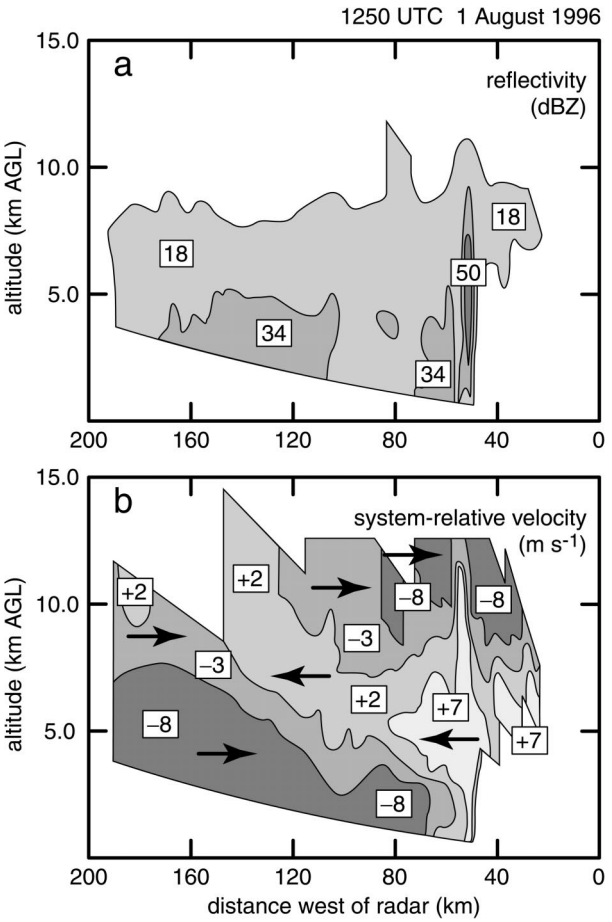

FIG. 16. Cross section of level II data through the middle of the mature MCS at 1250 UTC 1 Aug 1996. Panels show (a) regions of reflectivity enclosed by contours of 18, 34, and 50 dBZ; and (b) regions of system-relative radial wind enclosed by contours of 8 and 3 m s^{-1} toward the radar (west-northwesterlies), and 2 and 7 m s^{-1} away from the radar (east-southeasterlies). The section was taken along the 300° radian.

Most of the mesoscale perturbation in wind in the leading anvil was away from the convective line (Figs. 11d and 13a). This perturbation was reinforced by synoptic northwesterlies, relative to the system, in the upper troposphere (Fig. 16). Advections of hydrometeors by the relative total wind were no doubt responsible for the leading anvil. However, near the base of the cloud at about 6 km AMSL, both the perturbation in wind and the total wind were toward the convective line, not away from it. Such a collocation of leading anvil with rearward flow was explained by Smull and Houze (1985). They found that hydrometeors that are advected ahead of a convective line in RTF outflow can fall into FTR inflow, which advects the hydrometeors back toward the convective line.

The magnitude of the mesoscale perturbation in wind was asymmetric about the major axis of the MCS (across-line asymmetry) at some altitudes. In the lower and middle troposphere, the mesoscale perturbation in

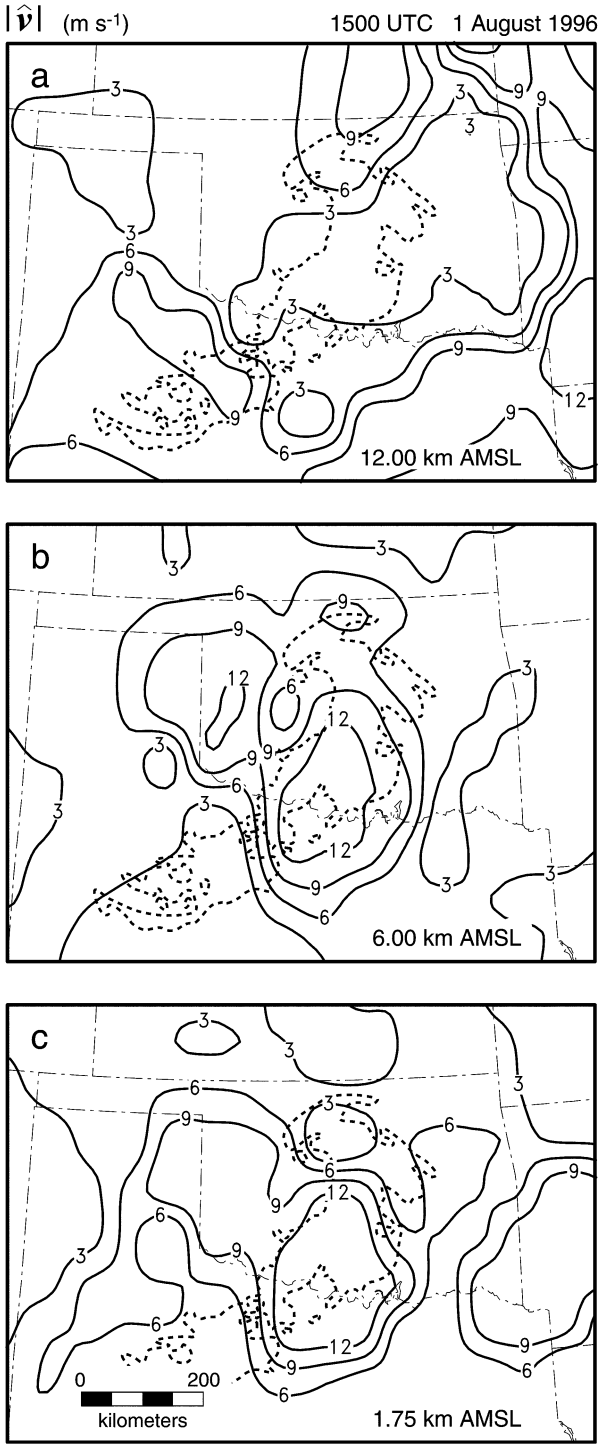

FIG. 17. Speed (m s^{-1}) of the mesoscale perturbation in wind at 1500 UTC 1 Aug 1996 at (a) 12.00, (b) 6.00, and (c) 1.75 km AMSL. The contour of 15-dBZ reflectivity within the MCS is dashed.

wind covered a larger area behind the stratiform region than ahead of the convective line (Figs. 17b,c). In particular, at 6.0 km AMSL a mesoscale perturbation in wind faster than 6 m s^{-1} extended farther than 300 km behind the back edge of the stratiform region's reflectivity (Fig. 17b). This was mainly the mesoscale downdraft. In the lower troposphere, the mesoscale perturbation in wind displayed a similar across-line asymmetry. However, in the upper troposphere, the across-line asymmetry was reversed in some cases (Fig. 17a), or, at times for which figures are not shown, the flow was generally symmetric. According to Pandya and Durran (1996), Nachamkin and Cotton (2000), and others, such altitude-dependent asymmetries are symptoms of vertical shear's ability to tilt and horizontally arrange heating and cooling in an MCS. In particular, Pandya and Durran found that in their simulated squall line a deep, rearward-leaning heat source trailed by a heat sink focused the most low-frequency energy in the direction of that tilt. The possibility that some of the perturbation in wind depicted in Fig. 17 was due to cumulonimbi unrelated to the MCS of 1 August 1996 cannot be ruled out, but we do not think the effect was great. The two largest masses of cumulonimbi that were closest to the MCS were in northeastern Kansas and Louisiana (not shown), quite far from the system.

c. Vertical wind shear

Between 1100 and 1700 UTC, as the MCV strengthened and the MCS declined and began to dissipate, both the mesoscale shear and the total shear through the lower part of the vortex (2.0–6.0 km AGL) decreased for a time (solid lines in Figs. 18a,b). The most precipitous decreases were between 1100 and 1300 UTC, when the convective line began to weaken and the second notch deformed the back edge of the stratiform precipitation. During these 2 h the MCV deepened substantially; the top of the column of positive vorticity rose from approximately 5.5 km AGL to higher than 9.0 km AGL (not shown). It is possible that the decrease in mesoscale shear was partly because wind became more vortical at increasing altitudes. The direction of the wind would have become more vertically uniform, but only if the MCV were not greatly tilted, which could not be confirmed. After 1700 UTC, the mesoscale shear began to increase in the lower and middle troposphere, perhaps as the vortical flow in the MCV began to lose coherence. The synoptic shear between 2.0 and 6.0 km AGL changed only slightly during the MCV's maturity (dot–dashed line in Fig. 18a), so the change in the total shear (solid line in Fig. 18b) was due mostly to mesoscale effects.

Overall reductions in the mesoscale and synoptic vertical shear between 0.5 and 2.5 and between 2.0 and 6.0 km AGL during the period of detailed analysis were interrupted by brief increases. Some single-hour spikes in mesoscale shear, such as at 1100 UTC (dashed and solid lines in Fig. 18a), probably resulted from the NPN's inconsistent sampling of the MCS. However, inconsistent sampling does not explain the prolonged local maximum in lower-tropospheric synoptic shear from

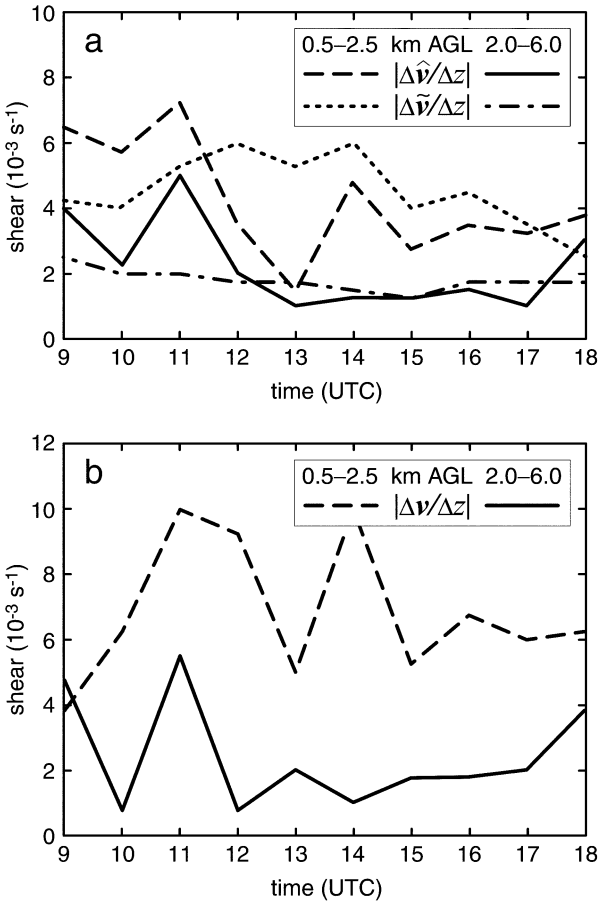

FIG. 18. Vertical wind shear (10^{-3} s^{-1}) from 0900 to 1800 UTC 1 Aug 1996 at the center of the MCV. Shears are (a) in the lower troposphere (0.5–2.5 km AGL) for the mesoscale perturbation in wind (dashed) and synoptic wind (dotted); in the middle troposphere (2.0–6.0 km AGL) for the same components (solid and dash–dotted, respectively); and (b) in the lower (dashed) and middle (solid) troposphere for the total wind. Each value is for a point, not an area.

1000 to 1400 UTC (dotted line in Fig. 18a). The short-wave trough, not the MCS, appeared to be responsible for this sustained increase. As it moved through the densest part of the NPN, the trough turned synoptic wind at 2.5 km AGL sharply from westerly to northwesterly (not shown). Then after the trough passed, synoptic shear in the lower troposphere decreased.

If the effects of the short-wave trough are discounted, synoptic shear in both the lower and middle troposphere decreased slightly overall through the period of detailed analysis. This suggests that as the MCS matured it may have altered the kinematics of its environment in a way that increasingly favored an MCV; Davis and Weisman (1994) and Trier et al. (2000b) showed that MCVs are more likely in weakly sheared rather than strongly sheared environments. However, the evidence is marginal, and factors other than the MCS may have reduced the synoptic shear as well.

The fact that over the entire period of detailed analysis shears in the mesoscale wind were generally as large as those in the synoptic wind suggests the need to reevaluate how the kinematical environments of MCVs are diagnosed. An average of environmental soundings outside an MCS probably does not accurately represent the shear that affects an MCV generated by that MCS. Because organized convective systems create their own circulations, the shear an MCV experiences must be a combination of environmental shear and system-scale shear.

6. Average kinematics over the MCV

Data from the NPN averaged over 3 h and over a 2° × 2° area centered on the MCV reveal the persistent circulations in total wind that shaped the MCS (Fig. 19). These persistent circulations were the mesoscale updraft and downdraft that met in a layer of convergence in the middle troposphere, divergent outflows in both the lower and upper troposphere, and the MCV. (References to *vertical velocity*, *divergence*, and *vorticity* in this section are to the temporal and spatial averages of those fields, unless otherwise stated.)

Profiles of vertical velocity, divergence, and vorticity for the total wind centered on the MCV are generally similar to such profiles in other studies (e.g., Brandes 1990; Scott and Rutledge 1995). We address differences where appropriate.

One consistent result among studies of MCSs is that the magnitudes of kinematical terms calculated over stratiform regions depend on whether data are fine or coarse and on how those data are averaged. Fine data and minimal averaging lead to high magnitudes. For example, some researchers have calculated middle-tropospheric maxima in vorticity within stratiform regions to be of order 1×10^{-6} s^{-1} [e.g., Cotton et al. (1989), with composites of semidaily operational soundings], others have calculated maxima 100 times larger [e.g., Chong and Bousquet (1999), with airborne Doppler data]. Our calculations are much closer to the latter than to the former.

a. Vertical velocity

The mesoscale updraft preceded the mesoscale downdraft (cf. dotted lines in Figs. 19a and 19b). This is because in the archetypal MCS—and in the MCS of 1 August 1996—mechanisms that accelerate a mesoscale updraft appear before mechanisms that accelerate a mesoscale downdraft (see section 1a). A mesoscale updraft originates primarily from the convective line. A mesoscale downdraft originates from a combination of the convective line and the stratiform region, including the cold pool in the lower troposphere beneath the trailing anvil. An expansive stratiform region and cold pool often do not appear until 4–8 h into the life of an MCS (Smull and Houze 1985). Cotton et al. (1989) found that

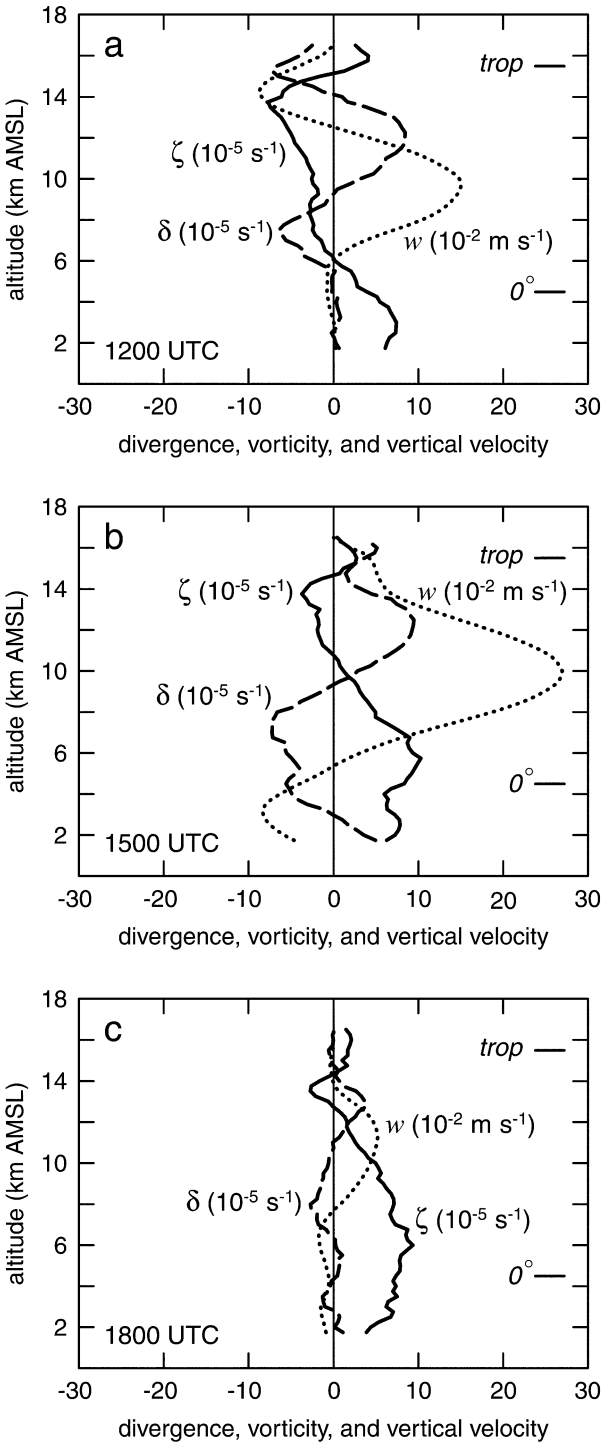

FIG. 19. Relative vorticity (solid in 10^{-5} s^{-1}), divergence (dashed in 10^{-5} s^{-1}), and vertical velocity (dotted in 10^{-2} m s^{-1}) of the total wind on 1 Aug 1996. Profiles are for a 2° × 2° area centered on the MCV, averaged over 3 h ending at the time labeled. Data below 1750 m AMSL are not plotted. The levels of 0°C in the environment and of the tropopause are marked along the right side of each panel.

a mesoscale downdraft did not exist much before the mature stage of their composite MCS.

By the time vorticity in the MCV of 1 August 1996 reached its maximum at 1500 UTC, both mesoscale drafts were present and at their strongest (Fig. 19b). The temporally and spatially averaged maximum velocity of the mesoscale updraft was nearly 30 cm s^{-1}; the mesoscale downdraft reached an average velocity of nearly −10 cm s^{-1}. As mentioned in section 1a, ascent in a mesoscale updraft is due to positively buoyant, dissipating cells from a convective line, and from heating by exothermic phase changes of water within the mesoscale updraft. Although the contour interval of 15 dB*Z* in Fig. 8 does not illustrate it, between 1200 and 1500 UTC the stratiform region contained large and persistent areas of enhanced reflectivity between 40 and 45 dB*Z*, a sign that hydrometeors were growing and heating the mesoscale updraft (Biggerstaff and Houze 1991), even though the MCS as a whole was dissipating. The mesoscale downdraft strengthened at 1500 UTC when erosion of the back edge of the stratiform rain signified the mechanisms that drive descent in such drafts: sublimative and evaporative cooling (Rutledge et al. 1988).

An additional indication that microphysics were important in forcing the two mesoscale drafts is that the average altitude that divided descent from ascent in the stratiform region (5.25 km AMSL) and the average altitude of 0°C in the environment (4.40 km AMSL) differed by only 0.85 km (Fig. 19b). This difference is near the midpoint of the commonly observed range of 0 to 2 km (Houze 1993).

Between 1500 and 1800 UTC, changes in the mesoscale drafts are not accurately portrayed in the spatial and temporal averages. Both drafts seem to have been present, although weak (Fig. 19c), which is not consistent with other studies in which mesoscale updrafts disappeared and mesoscale downdrafts deepened and persisted in late stages of MCSs that contained MCVs (e.g., Brandes 1990; Scott and Rutledge 1995). The explanation for the apparent inconsistency is that data from 1800 UTC distorted the average profile in Fig. 19c, either because they included convective updrafts from the fresh cumulonimbi that developed in the spiral rain bands, or because of the falloff in density of reporting wind profilers in eastern Oklahoma. Both are possible. The areally averaged profile of vertical motion at 1700 UTC alone—not averaged over 3 h—is qualitatively almost identical to profiles in the other studies mentioned: there was no mesoscale updraft, and the top of the mesoscale downdraft was at about 11 km AMSL (Fig. 20b).

b. Divergence

The magnitude of divergence was conspicuously small through the depth of the MCV between 0900 and 1200 UTC (dashed line in Fig. 19a), which suggests that tilting may have played a prominent role in the initial

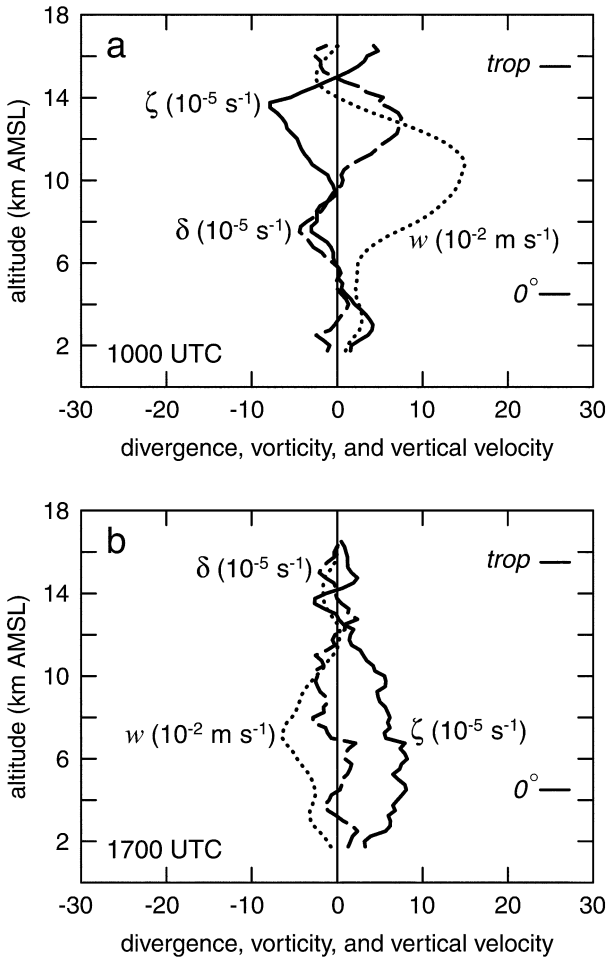

FIG. 20. Relative vorticity (solid in 10^{-5} s^{-1}), divergence (dashed in 10^{-5} s^{-1}), and vertical velocity (dotted in 10^{-2} m s^{-1}) of the total wind at (a) 1000 and (b) 1700 UTC 1 Aug 1996. Profiles are for a 2° × 2° area centered on the MCV. Unlike in Fig. 19, profiles are not for 3-h averages. Data below 1750 m AMSL are not plotted. The levels of 0°C in the environment and of the tropopause are marked along the right side of each panel.

formation of the MCV. Unfortunately, at the time the MCV first appeared it was well northwest of the part of the NPN sufficiently dense for detailed analysis, so the source of initial vorticity could not be determined. In an MCV simulated by Zhang (1992), a vortex whose final strengthening was mainly from convergence—as was the case with the MCV of 1 August 1996—did, in fact, begin mainly as tilted horizontal vorticity. (The results of a scale-discriminating vorticity budget for the MCV of 1 August 1996 will appear in an upcoming paper.)

Above the growing MCV lay convergence centered at 7.5 km and strong divergence centered at 12.0 km AMSL (Fig. 19a). Divergence in the upper troposphere, which persisted at various strengths over the entire period of analysis (Figs. 19a–c), is partially the signature of upper tropospheric high pressure that is a fundamental feature of MCSs in general, not just of those that generate MCVs (see section 1a).

At 1500 UTC (Fig. 19b), the vertical distribution of divergence was qualitatively identical to that calculated by Cotton et al. (1989) for the average stratiform region of a composite MCS (their Fig. 12). In the MCS of 1 August 1996, divergence first appeared in the lower troposphere, below about 3 km AMSL. It was equated with overturning and diffluence in the mesoscale downdraft as it neared the ground, or perhaps as it neared the top of stable air in the cold pool. The middle troposphere above was convergent where the horizontally opposed mesoscale up- and downdrafts met. The profile of divergence in the upper troposphere centered at about 12 km AMSL was nearly identical to that from 3 h earlier (cf. Figs. 19a and 19b). The vertical distribution of divergence at 1500 UTC was also consistent with buoyancy rolls generated by a combination of convective and stratiform heating, which Mapes (1993) illustrated. Divergence in the lower and upper troposphere may have been the outgoing branches of the $l = 2$ roll in his Fig. 6, and convergence in the middle troposphere may have been the incoming branch.

Divergence, both positive and negative, weakened markedly throughout the troposphere during the final 3 h of analysis (Fig. 19c). Maximum divergence rose in altitude as the MCS dissipated, a trend also apparent in figures by Cotton et al. (1989) and Brandes (1990). Upper-tropospheric divergence persisted, although it was considerably weaker than 3 h earlier. This weakening is substantially different from the dramatic increase in divergence within the declining composite MCS of Cotton et al. (1989). However, other studies specifically of MCSs that generated MCVs show trends in divergence more like we found (e.g., Brandes 1990; Chong and Bousquet 1999; Bousquet and Chong 2000). We reject the possibility that poor sampling by the NPN may have left undetected a spike in upper-tropospheric divergence because there was no pronounced falloff in detected vorticity within the MCV during the last 3 h of analysis (cf. Figs. 19b,c).

c. Vorticity

Over the period of detailed analysis, the MCV deepened and strengthened as the MCS matured and dissipated, until the vortex occupied almost the entire troposphere (solid lines in Fig. 19). According to the Oklahoma Mesonet, the MCV appeared even to reach the ground; by 1900 UTC a broad vortical circulation was centered at the back edge of the southern spiral band of the declining MCS (Fig. 21).

Two features in Fig. 21 are signs that the MCV may not have been highly tilted. First, the center of circulation at the ground at 1900 UTC was very near the center of circulation in the middle troposphere (the gray circle in the figure). Second, no pronounced mesoscale low appeared near the MCV—the low in western

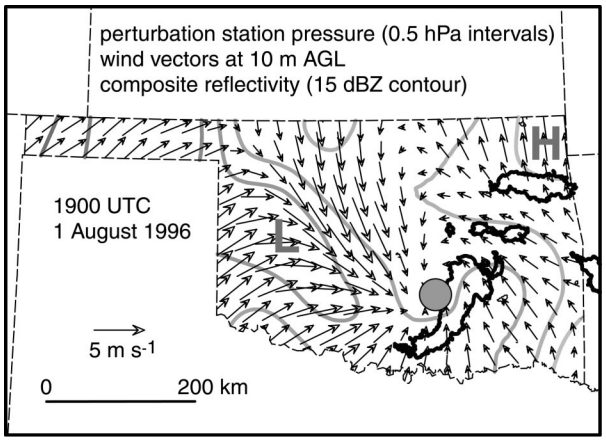

FIG. 21. Radar reflectivity and surface conditions within the Oklahoma Mesonet at 1900 UTC 1 Aug 1996. Surface pressure is contoured every 0.5 hPa in gray; values are deviations from a statewide mean and darker grays indicate lower pressure. Vectors depict wind at 10 m AGL. The thick black contours outline reflectivity $\geq$15 dBZ. The gray circle marks the middle-tropospheric center of the MCV.

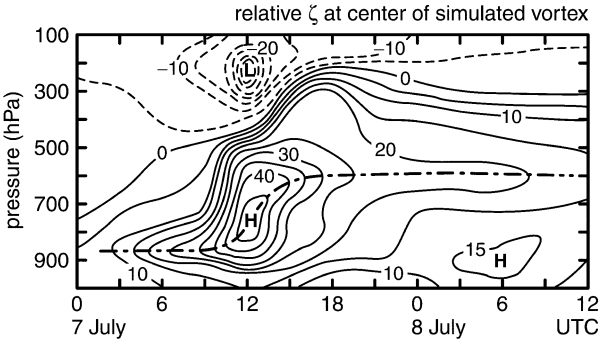

FIG. 22. Temporal change in maximum relative vertical vorticity in the numerically simulated MCV of 6–7 Jul 1982. Contours are every 5×10^{-5} s^{-1}. Negative contours are dashed. [Adapted from a figure by Zhang and Fritsch (1988).]

Oklahoma was most likely a vestigial wake low of the kind described by Johnson and Hamilton (1988), Loehrer and Johnson (1995), and Knievel and Johnson (1998). Highly tilted MCVs are more likely to generate mesoscale lows and highs at the ground because the warm air in the upper part of a tilted MCV's core is horizontally offset from the cold air in the lower part of the core, which means that perturbations in mass equated with the two perturbations in temperature do not vertically cancel.

Not only did the top and, perhaps, the bottom of the MCV change altitude with time, so did the maximum in vorticity. Positive vorticity in the vortex originated at about 3 km AMSL (Fig. 20a), the altitude of its average maximum from 0900 to 1200 UTC (Fig. 19a). The top of the MCV and the level of maximum vorticity both ascended between 1200 and 1500 UTC as the vortex strengthened (Fig. 19b). Then the height of maximum vorticity remained approximately fixed at 6 km AMSL for the remainder of the period of detailed analysis (Fig. 19c). The long-lived simulated MCV of Zhang and Fritsch (1988) behaved similarly: the height of maximum vorticity varied little for the first 2 h of the MCV's lifetime, rose abruptly as the MCV strengthened, then varied little after that (Fig. 22). Rogers and Fritsch (2001) simulated an MCV whose vorticity maximum ascended with time, even while the base of the vortex descended to the ground. Conversely, Chen and Frank (1993) simulated an MCV whose vorticity maximum descended, not ascended, with time. Few empirical studies recount temporal variations of vorticity within an MCV, but, among these few, Menard and Fritsch (1989) and Johnson and Bartels (1992) did find that maxima in vorticity ascended with time in two MCVs. [The MCV of 6–7 July 1982, which Menard and Fritsch studied, was the same MCV simulated by Zhang and Fritsch (1988)]. These and other studies (e.g., Zhang 1992; Davis and Weisman 1994) strongly suggest the intriguing possibility that some MCVs' life cycles can be divided into stages that are characterized by dominant sources of vorticity concentrated at distinctive altitudes. If so, a sudden ascent or descent of maximum vorticity within an MCV may signal a transition from one of these stages to another.

It is not surprising that the MCV of 1 August 1996 grew stronger even while the MCS declined. Although the strength and areal extent of radar echoes in the convective line decreased beginning as early as 1145 UTC, the stratiform region remained vigorous until 1430 UTC (Fig. 8), with large patches of reflectivity greater than 40 dBZ. When single, large, cyclonic MCVs are generated by diabatic heating in MCSs, it is generally heating by the stratiform region, not by the convective line, that is responsible (Hertenstein and Schubert 1991). When Zhang (1992) simulated the MCS of 10–11 June 1985, he, too, found that the MCV generated by that system grew stronger as the system declined. Indeed, the kinematical profiles from the declining stage of Zhang's system match quite closely the kinematical profiles for the same stage of the MCV of 1 August 1996 (cf. Figs. 19b and 23; note that Zhang depicted vertical velocity in units of pressure, not altitude).

The great depth of the MCV from 1500 to 1800 UTC has precedence. The simulated MCV of Chen and Frank (1993) had a top near 200 hPa, which would be 12.4 km AMSL in our case. Observed MCVs of Brandes (1990) and Bousquet and Chong (2000) had tops near 11 km AMSL.

The shallow, weak, negative vorticity above the MCV of 1 August 1996 is the signature of planetary vorticity's effect on divergent outflow from high pressure in the upper troposphere (Figs. 19 and 20). Others have also noted such a feature (e.g., Brandes 1990; Johnson and Bartels 1992; Bousquet and Chong 2000).

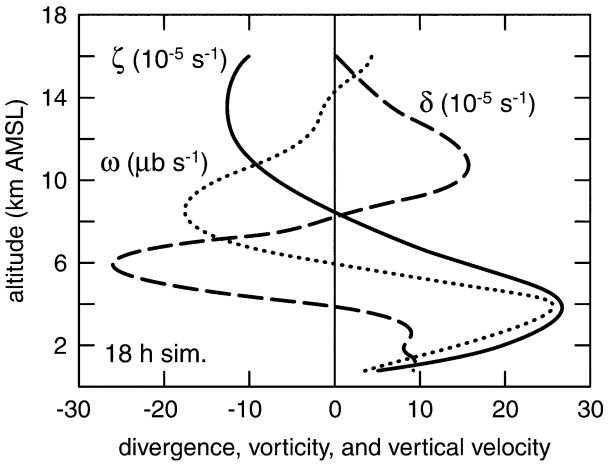

FIG. 23. Kinematical averages in the numerically simulated MCV of 10–11 Jun 1985. Profiles are for the mature stage of the MCV and the declining stage of the MCS. Relative vorticity (10^{-5} s^{-1}) is solid, divergence (10^{-5} s^{-1}) is dashed, and vertical velocity (μb s^{-1}) is dotted. Profiles are for a 100 km $\times$ 100 km area centered on the MCV after an 18-h simulation. [Adapted from a figure by Zhang (1992).]

7. Synthesis

We presented a unique, scale-discriminating study of the environment-relative circulations within a mesoscale convective system (MCS) and its mesoscale convective vortex (MCV). The environment-relative frame of reference is familiar to modelers (e.g., Pandya and Durran 1996; Pandya et al. 2000; Nachamkin and Cotton 2000), but empiricists almost never adopt it.

The MCS, which comprised a leading convective line and trailing stratiform region, traversed Kansas and Oklahoma on 1 August 1996 and displayed many of the features in radar reflectivity common to systems that generate MCVs: early along-line symmetry followed by asymmetry during maturity and decline; enhanced reflectivity in the stratiform region, which twice became notched due to one or more rear inflow jets; and spiral bands of weakly raining clouds as the MCS dissipated.

The environment of the MCS was typical of environments of MCSs in other studies. A synoptic ridge lay to the west of the system, and a trough lay to the east. Vorticity advection was weak. Wind was weakly to moderately sheared and veered from southeasterly near the ground to west-northwesterly in the middle and upper troposphere. Although a low-level jet was present, gradients in temperature and moisture were small so advections were weak. Mesoscale and synoptic fronts existed in the areas in which the MCS formed and moved.

Because the MCS matured, declined, and dissipated in the National Oceanic and Atmospheric Administration (NOAA) Profiler Network (NPN), we were able to analyze the kinematics of the MCS and MCV over 9 h on scales between those of semidaily operational rawinsondes and Doppler radars. We used a Barnes bandpass filter to divide observed wind into a component that was predominantly synoptic background wind and a component that was predominantly a mesoscale perturbation on that background wind.

The mesoscale, environment-relative wind was distributed asymmetrically about the major axis of the MCS; in the middle troposphere the wind extended farther behind the MCS than ahead of it, which is consistent with analytic studies and numerical simulations of gravity waves generated by heat sources in leading convective lines and trailing stratiform regions (Pandya and Durran 1996; Nachamkin and Cotton 2000). Within the asymmetrically distributed mesoscale wind were the four primary circulations commonly observed in MCSs: a rear-to-front (RTF) mesoscale downdraft and a front-to-rear (FTR) mesoscale updraft that horizontally converged in the middle troposphere, as well as divergent outflows in the lower and upper troposphere. Because these flows remained even after removal of the synoptic background wind we judged them to be internal and fundamental to the MCS, in agreement with numerous numerical simulations (e.g., Pandya and Durran 1996; Pandya et al. 2000; Nachamkin and Cotton 2000).

The MCV appeared as a nearly closed circulation within the middle-tropospheric mesoscale wind. At lower and higher altitudes, the resolved circulation was generally not quite closed, but we believe this was at least partly due to the resolution of the data. By the end of the 9 h of detailed analysis, the top of the MCV had reached to within a few kilometers of the tropopause, and the bottom had descended to below the lowest data available from the NPN. Data from the Oklahoma Mesonet suggest a vortical circulation may even have reached the ground while the MCS was declining.

Deepening of the MCV appeared to be reflected in the vertical wind shear at the vortex's center: as the MCV strengthened and the MCS declined and began to dissipate, the mesoscale shear through the lower part of the vortex decreased for a time, perhaps as wind became more vortical at increasing altitudes. Vertical shears in the mesoscale and synoptic wind were of similar magnitude over the period of detailed analysis, so an average of environmental soundings outside an MCS probably does not accurately represent the shear that affects an MCV generated by that MCS. Because organized convective systems create their own circulations, the shear an MCV experiences must be a combination of environmental shear and system-scale shear. This suggests the need to reevaluate how the kinematical settings of MCVs are diagnosed.

Together, the simple bandpass filter used and data from the NPN are powerful tools for studying mesoscale components of phenomena the size of MCVs and MCSs or larger. Unfortunately, if this study is representative, missing reports from even a few profilers at key times and locations can undermine detailed, hourly analyses. Meaningful results are still possible through temporal and spatial averaging or through space–time conver-

sions, which we did not use, but these approaches are not entirely satisfying. The real utility of the NPN lies in its *hourly* kinematical soundings, so missing data—especially when rain is the culprit—pose a problem for profiler-based studies of MCSs and MCVs. Operational alternatives to profiler soundings do exist, but so far none offers both the four-dimensional resolution and the synoptic spatial coverage of the NPN. Cloud-drift and water-vapor winds can be inferred from satellite images, but only at altitudes where there are trackable features. Dual-Doppler analyses of data from WSR-88Ds offer high vertical resolution, but only at times and locations where neighboring radars sample the same precipitation nearly simultaneously at appropriate ranges and angles. Sufficiently accurate velocity–azimuth display (VAD) analyses are also possible, but only when precipitation is nearly continuous, and not highly convective, in a ring around a radar. Finally, soundings from the Aircraft Communication Addressing and Reporting System (ACARS) are adequately resolved in the vertical, but in the lower and middle troposphere are extremely limited in horizontal coverage.

We are currently preparing another paper on the MCS and MCV of 1 August 1996. In that paper, too, we will take advantage of the rich dataset from the NPN and of the bandpass filter to present a vorticity budget that traces the origins of vorticity in the MCV to sources within both the synoptic background wind and the mesoscale perturbation in wind.

Acknowledgments. The National Science Foundation and the National Aeronautics and Space Administration supported this research with the respective Grants ATM 9618684 and NCC5-288 SUPP 0002.

Profiler data and code to read them are from Stan Trier and Chi-Fan Shih of the National Center for Atmospheric Research (NCAR); satellite images are from the Cooperative Institute for Research in the Atmosphere, thanks to Kelly Dean and Nan McClurg; the skew *T*–log *p* program is from Greg Thompson of NCAR; WSI's NOWrad radar reflectivity is from the Global Hydrology Resource Center; mesonetwork data are from the Oklahoma Climatological Survey; GCIP/ESOP-96 data are from the Joint Office for Scientific Support of the University Corporation for Atmospheric Research and the National Oceanic and Atmospheric Administration; and level II Doppler data are from NCAR, thanks to Stan Trier.

Contributions from the following people improved our research: Chris Davis and Stan Trier of NCAR; Charles Doswell III, Matt Gilmore, Tom Matejka, and Harald Richter of the National Severe Storms Laboratory; Steve Weygandt of the Forecast Systems Laboratory; Jason Nachamkin of the Naval Research Laboratory; William Cotton, Patrick Haertel, Scott Hausman, Jim Kossin, Brian McNoldy, Michael Montgomery, Matthew Parker, Walt Petersen, and Jorge Ramirez of CSU; and two anonymous reviewers. Matthew Parker, in particular, was extremely helpful. Rick Taft of CSU provided invaluable computer support.

REFERENCES

Barnes, S. L., 1973: Mesoscale objective analysis using weighted time-series observations. NOAA Tech. Memo. ERL NSSL-62, 60 pp. [NTIS COM-73-10781; also available from National Severe Storms Laboratory, Norman, OK 73069.]

Bartels, D. L., and R. A. Maddox, 1991: Midlevel cyclonic vortices generated by mesoscale convective systems. *Mon. Wea. Rev.,* **119,** 104–118.

Barth, M. F., R. B. Chadwick, and D. W. van de Kamp, 1994: Data processing algorithms used by NOAA's wind profiler demonstration network. *Ann. Geophys.,* **12,** 518–528.

Biggerstaff, M. I., and R. A. Houze Jr., 1991: Kinematic and precipitation structure of the 10–11 June 1985 squall line. *Mon. Wea. Rev.,* **119,** 3034–3065.

Bosart, L. F., and F. Sanders, 1981: The Johnstown flood of July 1977: A long-lived convective storm. *J. Atmos. Sci.,* **38,** 1616–1642.

Bousquet, O., and M. Chong, 2000: The oceanic mesoscale convective system and associated mesovortex observed 12 December 1992 during TOGA-COARE. *Quart. J. Roy. Meteor. Soc.,* **126,** 189–211.

Brandes, E. A., 1990: Evolution and structure of the 6–7 May 1985 mesoscale convective system and associated vortex. *Mon. Wea. Rev.,* **118,** 109–127; Corrigendum, **118,** 990.

——, and C. L. Ziegler, 1993: Mesoscale downdraft influences on vertical vorticity in a mature mesoscale convective system. *Mon. Wea. Rev.,* **121,** 1337–1353.

Brock, F. V., K. C. Crawford, R. L. Elliott, G. W. Cuperus, S. J. Stadler, H. L. Johnson, and M. D. Eilts, 1995: The Oklahoma Mesonet: A technical overview. *J. Atmos. Oceanic Technol.,* **12,** 5–19.

Brown, J. M., 1979: Mesoscale unsaturated downdrafts driven by rainfall evaporation: A numerical study. *J. Atmos. Sci.,* **36,** 313–338.

Ceselski, B. F., and L. L. Sapp, 1975: Objective wind field analysis using line integrals. *Mon. Wea. Rev.,* **103,** 89–100.

Chen, S. S., and W. M. Frank, 1993: A numerical study of the genesis of extratropical convective mesovortices. Part I: Evolution and dynamics. *J. Atmos. Sci.,* **50,** 2401–2426.

Chong, M., and O. Bousquet, 1999: A mesovortex within a near-equatorial mesoscale convective system during TOGA COARE. *Mon. Wea. Rev.,* **127,** 1145–1156.

Cotton, W. R., M. S. Lin, R. L. McAnelly, and C. J. Tremback, 1989: A composite model of mesoscale convective complexes. *Mon. Wea. Rev.,* **117,** 765–783.

Davis, C. A., and M. L. Weisman, 1994: Balanced dynamics of mesoscale vortices produced in simulated convective systems. *J. Atmos. Sci.,* **51,** 2005–2030.

Durran, D. R., and J. B. Klemp, 1982: On the effects of moisture on the Brunt–Väisälä frequency. *J. Atmos. Sci.,* **39,** 2152–2158.

Emanuel, K. A., 1983: The dynamical definitions of ''mesoscale.'' *Mesoscale Meteorology—Theories, Observations, and Models,* D. K. Lilly and T. Gal-Chen, Eds., Reidel, 1–11.

Fortune, M. A., W. R. Cotton, and R. L. McAnelly, 1992: Frontal-wave–like evolution in some mesoscale convective complexes. *Mon. Wea. Rev.,* **120,** 1279–1300.

Frank, W. M., 1983: The cumulus parameterization problem. *Mon. Wea. Rev.,* **111,** 1859–1871.

Fritsch, J. M., J. D. Murphy, and J. S. Kain, 1994: Warm-core vortex amplification over land. *J. Atmos. Sci.,* **51,** 1780–1807.

Fujita, T. T., 1981: Tornadoes and downbursts in the context of generalized planetary scales. *J. Atmos. Sci.,* **38,** 1511–1534.

Gallus, W. A., Jr., and R. H. Johnson, 1992: The momentum budget of an intense midlatitude squall line. *J. Atmos. Sci.,* **49,** 422–450.

Harr, P. A., M. S. Kalafsky, and R. L. Elsberry, 1996: Environmental

conditions prior to formation of a midget tropical cyclone during CTM-93. *Mon. Wea. Rev.*, **124,** 1693–1710.
Hertenstein, R. F. A., and W. H. Schubert, 1991: Potential vorticity anomalies associated with squall lines. *Mon. Wea. Rev.*, **119,** 1663–1672.
Hilgendorf, E. R., and R. H. Johnson, 1998: A study of the evolution of mesoscale convective systems using WSR-88D data. *Wea. Forecasting*, **13,** 437–452.
Houze, R. A., Jr., 1993: *Cloud Dynamics*. Academic Press, 573 pp.
——, S. A. Rutledge, M. I. Biggerstaff, and B. F. Smull, 1989: Interpretation of Doppler weather radar displays of midlatitude mesoscale convective systems. *Bull. Amer. Meteor. Soc.*, **70,** 608–619.
——, B. F. Smull, and P. Dodge, 1990: Mesoscale organization of springtime rainstorms in Oklahoma. *Mon. Wea. Rev.*, **118,** 613–654.
Johnson, R. H., and W. A. Gallus Jr., 1988: The wake structure of an intense midlatitude squall line in OK PRE-STORM. Preprints, *Eighth Conf. on Numerical Weather Prediction and 15th Conf. on Severe Local Storms*, Baltimore, MD, Amer. Meteor. Soc., 229–232.
——, and P. J. Hamilton, 1988: The relationship of surface pressure features to the precipitation and airflow structure of an intense midlatitude squall line. *Mon. Wea. Rev.*, **116,** 1444–1472.
——, and D. L. Bartels, 1992: Circulations associated with a mature-to-decaying midlatitude mesoscale convective system. Part II: Upper-level features. *Mon. Wea. Rev.*, **120,** 1301–1320.
——, W. A. Gallus Jr., and M. D. Vescio, 1990: Near-tropopause vertical motion within the trailing stratiform region of a midlatitude squall line. *J. Atmos. Sci.*, **47,** 2200–2210.
Knievel, J. C., and R. H. Johnson, 1998: Pressure transients within MCS mesohighs and wake lows. *Mon. Wea. Rev.*, **126,** 1907–1930.
Koch, S. E., M. DesJardins, and P. J. Kocin, 1983: An interactive Barnes objective map analysis scheme for use with satellite and conventional data. *J. Climate Appl. Meteor.*, **22,** 1487–1503.
LeMone, M. A., 1983: Momentum transport by a line of cumulonimbus. *J. Atmos. Sci.*, **40,** 1815–1834.
Ligda, M. G. H., 1951: Radar storm observation. *Compendium of Meteorology*, T. F. Malone, Ed., Amer. Meteor. Soc., 1265–1282.
Loehrer, S. M., and R. H. Johnson, 1995: Surface pressure and precipitation life cycle characteristics of PRE-STORM mesoscale convective systems. *Mon. Wea. Rev.*, **123,** 600–621.
Maddox, R. A., 1980: An objective technique for separating macroscale and mesoscale features in meteorological data. *Mon. Wea. Rev.*, **108,** 1108–1121.
——, D. J. Perkey, and J. M. Fritsch, 1981: Evolution of upper tropospheric features during the development of a mesoscale convective complex. *J. Atmos. Sci.*, **38,** 1664–1674.
Mapes, B. E., 1993: Gregarious tropical convection. *J. Atmos. Sci.*, **50,** 2026–2037.
Menard, R. D., and J. M. Fritsch, 1989: A mesoscale convective complex-generated inertially stable warm core vortex. *Mon. Wea. Rev.*, **117,** 1237–1261.
Miller, D., and J. M. Fritsch, 1991: Mesoscale convective complexes in the western Pacific region. *Mon. Wea. Rev.*, **119,** 2978–2992.
Nachamkin, J. E., and W. R. Cotton, 2000: Interactions between a developing mesoscale convective system and its environment. Part II: Numerical simulation. *Mon. Wea. Rev.*, **128,** 1225–1244.
Nicholls, M. E., R. A. Pielke, and W. R. Cotton, 1991: Thermally forced gravity waves in an atmosphere at rest. *J. Atmos. Sci.*, **48,** 1869–1884.
O'Brien, J. J., 1970: Alternative solutions to the classical vertical velocity problem. *J. Appl. Meteor.*, **9,** 197–203.
Orlanski, I., 1975: A rational subdivision of scales for atmospheric processes. *Bull. Amer. Meteor. Soc.*, **56,** 527–530.
Pandya, R. E., and D. R. Durran, 1996: The influence of convectively generated thermal forcing on the mesoscale circulation around squall lines. *J. Atmos. Sci.*, **53,** 2924–2951.
——, ——, and M. L. Weisman, 2000: The influence of convective thermal forcing on the three-dimensional circulation around squall lines. *J. Atmos. Sci.*, **57,** 29–45.
Parker, M. D., and R. H. Johnson, 2000: Organizational modes of midlatitude mesoscale convective systems. *Mon. Wea. Rev.*, **128,** 3413–3436.
Raymond, D. J., and H. Jiang, 1990: A theory for long-lived mesoscale convective systems. *J. Atmos. Sci.*, **47,** 3067–3077.
Rogers, R. F., and J. M. Fritsch, 2001: Surface cyclogenesis from convectively driven amplification of midlevel mesoscale convective vortices. *Mon. Wea. Rev.*, **129,** 605–637.
Rutledge, S. A., R. A. Houze Jr., M. I. Biggerstaff, and T. Matejka, 1988: The Oklahoma–Kansas mesoscale convective system of 10–11 June 1985: Precipitation structure and single-Doppler radar analysis. *Mon. Wea. Rev.*, **116,** 1409–1430.
Schaefer, J. T., and C. A. Doswell III, 1979: On the interpolation of a vector field. *Mon. Wea. Rev.*, **107,** 458–476.
Schubert, W. H., and J. J. Hack, 1982: Inertial stability and tropical cyclone development. *J. Atmos. Sci.*, **39,** 1687–1697.
——, ——, P. L. Silva Dias, and S. R. Fulton, 1980: Geostrophic adjustment in an axisymmetric vortex. *J. Atmos. Sci.*, **37,** 1464–1484.
Scott, J. D., and S. A. Rutledge, 1995: Doppler radar observations of an asymmetric MCS and associated vortex couplet. *Mon. Wea. Rev.*, **123,** 3437–3457.
Skamarock, W. C., M. L. Weisman, and J. B. Klemp, 1994: Three-dimensional evolution of simulated long-lived squall lines. *J. Atmos. Sci.*, **51,** 2563–2584.
Smull, B. F., and R. A. Houze Jr., 1985: A midlatitude squall line with a trailing region of stratiform rain: Radar and satellite observations. *Mon. Wea. Rev.*, **113,** 117–133.
——, and ——, 1987: Rear inflow in squall lines with trailing stratiform precipitation. *Mon. Wea. Rev.*, **115,** 2869–2889.
Trier, S. B., C. A. Davis, and W. C. Skamarock, 2000a: Long-lived mesoconvective vortices and their environment. Part II: Induced thermodynamic destabilization in idealized simulations. *Mon. Wea. Rev.*, **128,** 3396–3412.
——, ——, and J. D. Tuttle, 2000b: Long-lived mesoconvective vortices and their environment. Part I: Observations from the central United States during the 1998 warm season. *Mon. Wea. Rev.*, **128,** 3376–3395.
Weber, B. L., D. B. Wuertz, D. C. Welsh, and R. McPeek, 1993: Quality controls for profiler measurements of winds and RASS temperatures. *J. Atmos. Oceanic Technol.*, **10,** 452–464.
Whiteman, C. D., X. Bian, and S. Zhong, 1997: Low-level jet climatology from enhanced rawinsonde observations at a site in the southern Great Plains. *J. Appl. Meteor.*, **36,** 1363–1376.
Zhang, D.-L., 1992: The formation of a cooling-induced mesovortex in the trailing stratiform region of a midlatitude squall line. *Mon. Wea. Rev.*, **120,** 2763–2785.
——, and J. M. Fritsch, 1988: A numerical investigation of a convectively generated, inertially stable, extratropical warm-core mesovortex over land. Part I: Structure and evolution. *Mon. Wea. Rev.*, **116,** 2660–2687.
Zipser, E. J., 1977: Mesoscale and convective-scale downdrafts as distinct components of squall-line structure. *Mon. Wea. Rev.*, **105,** 1568–1589.